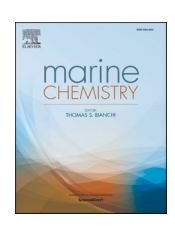
ELSEVIER

Contents lists available at ScienceDirect

Marine Chemistry

journal homepage: www.elsevier.com/locate/marchem





A half-cell reaction approach for pH calculation using a solid-state chloride ion-selective electrode with a hydrogen ion-selective ion-sensitive field effect transistor

S. Fisher Gonski ^{a,*}, George W. Luther III ^{a,*}, Amanda L. Kelley ^b, Todd R. Martz ^c, Elliott G. Roberts ^d, Xinyu Li ^{d,1}, Bo Dong ^d, Jordan A. Watson ^a, Taylor S. Wirth ^c, Najid Hussain ^d, Randy J. Feris Serrano ^a, Edward Hale ^{a,e}, Wei-Jun Cai ^d

- ^a School of Marine Science and Policy, University of Delaware, Lewes, DE 19958, USA
- ^b University of Alaska Fairbanks, College of Fisheries & Ocean Sciences, Fairbanks, AK 99775, USA
- ^c Scripps Institution of Oceanography, University of California San Diego, La Jolla, CA 92093, USA
- ^d School of Marine Science and Policy, University of Delaware, Newark, DE 19716, USA
- e Delaware Sea Grant, University of Delaware, Lewes, DE 19958, USA

ARTICLE INFO

Keywords: pH Ion selective electrode ISFET Sensor Acidification Potentiometry

ABSTRACT

Here, we explicitly define a half-cell reaction approach for pH calculation using the electrode couple comprised of the solid-state chloride ion-selective electrode (Cl-ISE) as the reference electrode and the hydrogen ion-selective ion-sensitive field effect transistor (ISFET) of the Honeywell Durafet as the hydrogen ion (H $^+$)-sensitive measuring or working electrode. This new approach splits and isolates the independent responses of the Cl-ISE to the chloride ion (Cl $^-$) (and salinity) and the ISFET to H $^+$ (and pH), and calculates pH directly on the total scale (pH $^{\rm EXT}_{\rm total}$) in molinity (mol (kg-soln) $^{-1}$) concentration units. We further apply and compare pH $^{\rm EXT}_{\rm total}$ calculated using the half-cell and the existing complete cell reaction (defined by Martz et al. (2010)) approaches using measurements from two SeapHOx sensors deployed in a test tank. Salinity (on the Practical Salinity Scale) and pH oscillated between 1 and 31 and 6.9 and 8.1, respectively, over a six-day period.

In contrast to established Sensor Best Practices, we employ a new calibration method where the calibration of raw pH sensor timeseries are split out as needed according to salinity. When doing this, pH_{total}^{EXT} had root-mean squared errors ranging between ± 0.0026 and ± 0.0168 pH calculated using both reaction approaches relative to pH_{total} of the discrete bottle samples (pH_{total}^{lisc}) . Our results further demonstrate the rapid response of the Cl-ISE reference to variable salinity with changes up to $\pm 12~(30~\text{min})^{-1}$. Final calculated pH_{total}^{EXT} were $\leq \pm 0.012~pH$ when compared to pH_{total}^{disc} following salinity dilution or concentration. These results are notably in contrast to those of the few in situ field deployments over similar environmental conditions that demonstrated pH_{total}^{EXT} calculated using the Cl-ISE as the reference electrode had larger uncertainty in nearshore waters. Therefore, additional work beyond the correction of variable temperature and salinity conditions in pH calculation using the Cl-ISE is needed to examine the effects of other external stimuli on in situ electrode response. Furthermore, whereas past work has focused on in situ reference electrode response, greater scrutiny of the ISFET as the H^+ -sensitive measuring electrode for pH measurement in natural waters is also needed.

^{*} Corresponding authors.

E-mail addresses: sfgonski@udel.edu (S.F. Gonski), luther@udel.edu (G.W. Luther).

Present address: Cooperative Institute for Climate, Ocean, and Ecosystem Studies, University of Washington, Seattle, WA 98195, USA.

Glossary of Terms and Abbreviations

Glossary of Te	and ribbleviations
A	Debye-Hückel constant.
$\mathbf{a_i}$	Activity of an ion on the molality (mol (kg-H ₂ O) ⁻¹) scale. a _H and
	a_{Cl} are the activities of hydrogen and chloride, respectively. Activity of an ion on the molinity (mol (kg-soln) ⁻¹) scale. $^{\kappa}a_{H}$ and
$\kappa_{\mathbf{a_i}}$	$^{\kappa}a_{\text{Cl}}$ are the activities of hydrogen and chloride, respectively, on
	the molality scale.
c_0	Sensor offset (or intercept) of a model II least square fit of two datasets of the same parameter (e.g., temperature or pH); the
- 0	ideal value is zero.
	Sensor gain (or slope) of a model II least square fit of two datasets
c_1	of the same parameter (e.g., temperature or pH); the ideal value is 1.
CC	Complete cell reaction approach.
	Solid-state chloride ion-selective electrode. Serves as the post-
Cl-ISE	factory added external reference electrode for pH measurement and calculation.
CRMs	Certified Reference Materials for DIC and TA analyses.
	Temperature dependence term of the calibration constant specific
$dE_{EXT}^*/dTemp$	to the Cl-ISE for the complete cell reaction approach (E_{EXT}^*) . Term has units of mV ${}^{\circ}C^{-1}$.
	Temperature dependence term of the calibration constant specific
dE* EXT hc/dTemp	to the Cl-ISE for the half-cell reaction approach $\left(E_{EXT,hc}^*\right)$. Term
EA1,it/	has units of mV ${}^{\rm o}{\rm C}^{-1}$.
DI water	Deionized water.
e	Charge of an electron; 1.602×10^{-19} C. Dielectric constant of H ₂ O or solution; unitless.
ε	Permittivity of free space; $8.8540 \times 10^{12} \text{ C}^2 \text{ N}^{-1} \text{m}^{-2}$ or
ϵ_0	$C^2 J^{-1} m^{-1}$.
E _{cell} or E _{EXT}	Voltage measured between the Cl-ISE as the reference electrode
E _{REF}	and ISFET as the H ⁺ -sensitive measuring or working electrode. Voltage measured by the Cl-ISE as the reference electrode.
	Voltage measured by the ISFET as the H ⁺ -sensitive measuring or
$\mathbf{E}_{\mathbf{work}}$	working electrode.
	Calibration constant specific to the Cl-ISE for the complete cell
\mathbf{E}_{cell}^* or \mathbf{E}_{EXT}^*	reaction approach. $E_{EXT}^*(t)$ is the value at <i>in situ</i> temperature. $E_{EXT}^*(t)$ is the value corrected to the reference temperature of
	25°C.
	Calibration constant specific to the Cl-ISE for the half-cell
$\mathbf{E}^*_{\mathbf{EXT.hc}}$	reaction approach. $E_{EXT,hc}^*(t)$ is the value at <i>in situ</i> temperature.
EAT,IR	$E_{EXT,hc,25}^*$ is the value corrected to the reference temperature of 25°C.
	Electrode standard potential for the electrode couple comprised
E _{cell} or E _{EXT}	of the Cl-ISE as the reference electrode and ISFET as the
$\mathbf{E}^{\mathrm{o}}_{\mathrm{RFF}}$	H ⁺ -sensitive measuring or working electrode.
	Reference electrode (Cl-ISE) standard potential. H ⁺ -sensitive measuring or working electrode (ISFET) standard
$\mathbf{E_{work}^o}$	potential.
F	Faraday Constant; 96,485 C mol ⁻¹ . Combined ion activity coefficient for Hydrogen Chloride (HCl) on
$\gamma_{\pm HCl}$ or $\gamma_H\gamma_{Cl}$	a molality (mol (kg- H_2O) ⁻¹ where H_2O is pure water) basis.
	Ion activity coefficient on a molality (mol (kg- H_2O) ⁻¹) basis
γ_{i}	where H_2O is pure water. γ_H and γ_{Cl} are the ion activity coefficients of hydrogen and chloride on a molality (mol (kg-
	$H_2O)^{-1}$) basis, respectively.
	Ion activity coefficient on a molinity (mol (kg-soln) 1) basis. $^{\kappa}\gamma_{H}$
$^{\kappa}\gamma_{i}$	and $^{\kappa}\gamma_{Cl}$ are the ion activity coefficients of hydrogen and chloride on a molinity (mol (kg-soln) ⁻¹) basis, respectively.
GOA-ON	Global Ocean Acidification Observing Network.
h	Hour.
HC I	Half-cell reaction approach. Ionic strength.
ISFET	Ion-sensitive field effect transistor.
κį	Molinity concentration in units of mol (kg-soln) $^{-1}$. κ_H and κ_{Cl} are
k _B	the molinities of hydrogen and chloride, respectively. Boltzmann Constant; $1.3807 \times 10^{23} \text{ J K}^{-1}$.
K _S	Bisulfate (HSO ₄) dissociation constant.
LPH	Liters per hour.
m	Molality concentration in units of mol (kg-H ₂ O) ⁻¹ where H ₂ O is
m _i	pure water. m_H and m_{Cl} are the molalities of hydrogen and chloride, respectively.
mCP	Purified meta-Cresol Purple indicator dye.
N_A	Avogadro's Number; 6.022 x 10 ²³ mol ⁻¹ .
Q	pH uncertainty of the discrete water samples propagated in quadrature.

(continued on next column)

(continued)

R	Gas Constant; 8.3145 J mol ⁻¹ K ⁻¹ .			
RMSE	Root-mean-square error.			
S	Nernst slope.			
ρ	Density at 1 atm in units of in kg- H_2O m ⁻³ or kg-soln m ⁻³ .			
pH_{total}	pH on the total scale.			
pH_{total}^{disc}	Discrete water sample pH _{total} corrected from 25°C to in situ			
- total	temperature.			
pH^{EXT}	Non-descript pH calculated using the Cl-ISE as the reference electrode.			
$\mathbf{p}\mathbf{H}^{\mathbf{EXT}}_{\mathbf{free}}$	pH on the free scale calculated using the Cl-ISE as the reference electrode.			
pH ^{EXT}	pH on the total scale calculated using the Cl-ISE as the reference electrode. An added superscript 'HC' or 'CC' denote the half-cell or complete reaction approaches, respectively. An added subscript 'single' or 'split' denote different sensor calibration methods where data were treated as single continuous timeseries or split out according to salinity as needed, respectively. For example, pH _{total,split} is pH _{total} calculated using the half-cell reaction approach where data were split out according to salinity as needed for sensor calibration.			
pH^{INT}	Non-descript pH measured using the internal Ag/AgCl reference.			
$\Delta p H_{total}$	Bottle pH anomaly between pH_{total}^{disc} and pH_{total}^{EXT} at the same timestamp.			
Salinity	Refers to salinity on the Practical Salinity Scale.			
$\left[SO_4^{2-} \right]_{total}$	Total concentration of sulfate (SO_4^{2-}) in solution.			
SP033/SP053	SeapHOx sensor S/Ns used to identify the sensors.			
SW	Seawater			
t	Temperature in degrees Celsius.			
T	Temperature in Kelvin.			
TA	Total Alkalinity in μ mol kg $^{-1}$.			
z	Charge of an ion.			

1. Introduction

The widespread application of commercially available autonomous sensors for pH measurement in dynamic nearshore waters characteristic, of estuarine and coastal systems, is encumbered by their extensive simultaneous ranges of and rates of change in pH, temperature, salinity, and other conservative and non-conservative water quality parameters (Gonski et al., 2023). Moreover, pH data records collected using either autonomous sensors or discrete water samples in estuarine and coastal systems remain scarce (e.g., Mucci et al. (2018)). Despite recent advancements in pH sensor development, marine technology, and ocean observation (Bagshaw et al., 2021; Chai et al., 2020; Mowlem et al., 2021; Nehir et al., 2022; Okazaki et al., 2017; Sastri et al., 2019; Velo and Padin, 2022), there is still an urgent need for robust and fast-responding pH sensors to resolve large, rapid biogeochemical changes and distinguish between long-term trends and natural variability in these systems.

A pH sensor technology that is filling this gap is the Honeywell Durafet Ion-Sensitive Field Effect Transistor (ISFET) technology (Martz et al., 2010; Bresnahan et al., 2014). The Durafet has been integrated into commercially available potentiometric pH sensors (e.g., SeaFET and SeapHOx, Sea-Bird Scientific, Bellevue, WA, USA). These sensors calculate and report a pair of pH values using its internal (Ag/AgCl reference – pH^{INT}) and post-factory added external (solid-state chloride ion-selective electrode, Cl-ISE – pH^{EXT}) reference electrodes (Martz et al., 2010). Durafet-based pH sensors have already demonstrated exceptional versatility through their widespread utilization in situ in both fixed point and mobile applications (Bresnahan et al., 2016, 2021; Duke et al., 2021; Johnson et al., 2016; Saba et al., 2019; Takeshita et al., 2021). Moreover, assessing the response and performance of Durafetbased pH sensors in dynamic estuarine and coastal systems is already an active area of research (Fritzsche et al., 2018; Gonski et al., 2018, 2023; McLaughlin et al., 2017; Miller et al., 2018, 2021).

The external CI-ISE that exhibits a Nernstian response to chloride ion activity in seawater (Takeshita et al., 2014) should ostensibly be an ideal reference electrode for pH^{EXT} measurement over dynamic environmental conditions in estuarine and coastal systems (Martz et al., 2010).

The Cl-ISE's small thermal mass enables more rapid thermal equilibration, and it also lacks a liquid junction (Martz et al., 2010; Bresnahan et al., 2014). Moreover, since activities and concentrations of major ions in seawater are known (Dickson et al., 2007; Stumm and Morgan, 1996), their existing thermodynamic functions can be leveraged to reflect variable environmental conditions to assist with pH calculation (Martz et al., 2010).

However, the performance of the Cl-ISE has only been reliably tested and verified in seawater media down to salinity 20 under rigorously controlled laboratory conditions (Takeshita et al., 2014). Furthermore, in situ Cl-ISE response in estuarine and coastal systems may also be complicated by long pre-deployment conditioning times (Bresnahan et al., 2014) and cross-sensitivity to interfering anions such as bromide (Br $^-$) and sulfide (S $^2-$) (Gonski et al., 2023; Takeshita et al., 2014). Estuarine field measurements calibrated to pH of coincident discrete samples collected alongside deployed sensors have already demonstrated that pH $^{\rm EXT}$, calculated using the Cl-ISE as the reference electrode, to be less reliable in natural waters of salinity <20 (Gonski et al., 2018, 2023). It is important to note, though, that shortcomings associated with the collection and analysis of discrete samples used to calibrate raw sensor pH can impart errors into pH $^{\rm EXT}$ timeseries (Bresnahan et al., 2021; Miller et al., 2021; Miller and Kelley, 2021).

In its current configuration, pH^{EXT} calculation using the Cl-ISE integrated with Durafet-based pH sensors is governed by the complete cell potential equation (Eq. (1) from Martz et al. (2010)), which on expansion gives Eq. (1a).

$$E_{cell} = E_{cell}^* - Slog_{10}(a_H a_{Cl}) = E_{cell}^* - Slog_{10}(\gamma_H \gamma_{Cl}) - Slog_{10}(m_H m_{Cl}) \tag{1} \label{eq:ecll}$$

is a clear need to develop and assess the suitability of a half-cell reaction approach for pH $^{\rm EXT}$ calculation using the Cl-ISE. Here, we describe and apply the half-cell reaction approach to calculate pH $^{\rm EXT}$ using the Cl-ISE from measurements made using two SeapHOx sensors (SP033 and SP053) over a six-day period in a test tank in June 2022 when salinity and pH were decreased and increased between 1 and 31 and 6.9 and 8.1, respectively. Herein, we also report the results of a detailed assessment of and comparison between pH $^{\rm EXT}$ calculated using the existing complete cell reaction and the new half-cell reaction approaches across a suite of dynamic environmental conditions to help inform and improve the utilization of the Cl-ISE as the reference electrode in estuarine and coastal systems in future work.

2. pHEXT Calculation

2.1. Complete cell (CC) reaction approach

The SeapHOx sensors (SP033 and SP053) used in the present work were originally assembled and tested at Scripps Institution of Oceanography. Accordingly, the equations describing the sensor's operating principle for the complete cell (CC) reaction approach follow those presented in Bresnahan et al. (2014) and Martz et al. (2010). pH^{EXT} is calculated using the complete cell reaction approach using a rearranged form of Eq. (1a) when the Cl-ISE acts as the reference electrode and the ISFET acts as the H^+ -sensitive measuring electrode given in Eq. (2).

$$pH^{EXT} = \frac{\left(E_{EXT} - E_{EXT}^*\right) + Slog_{10}(\gamma_H \gamma_{CI} m_{CI})}{S} \tag{2}$$

Here, pH^{EXT} is calculated on the free scale $\left(pH_{free}^{EXT}\right)$ in terms of molality

$$E_{cell} = E_{cell}^* - Slog_{10}(\gamma_H \gamma_{Cl} m_{Cl}) - Slog_{10}(m_H) = E_{cell}^* - Slog_{10}(\gamma_H \gamma_{Cl} m_{Cl}) - S pH^{EXT}$$
(1a)

Here, E_{cell} is the voltage measured by the electrochemical cell comprised of the Cl-ISE as the reference electrode and ISFET of the Honeywell Durafet as the H⁺-sensitive measuring electrode, E_{cell}^* is the calibration constant (similar to an electrode standard potential; described further in Martz et al. (2010) and section 2.2.1), a_i is the activity of hydrogen (H⁺) or chloride (Cl⁻), and γ_i and m_i are the ion activity coefficients and molalities, respectively, of H⁺ or Cl⁻. The electrode couple comprised of the Cl-ISE (reference electrode) and ISFET of the Honeywell Durafet (H⁺-sensitive measuring electrode) measures dissolved hydrogen chloride (HCl) directly in natural waters, so its electrochemical response is parameterized as the activity product of the hydrogen and chloride ions ($a_H a_{Cl}$) as in Eq. (1).

Equilibrium ion exchange between the electrode surfaces and overlying waters must be maintained as environmental conditions vary to preserve the electrode couple's Nernstian response to HCl. In the open ocean where pH and salinity remain relatively constant, this is not a problem (Bresnahan et al., 2014; Martz et al., 2010). In contrast, dynamic nearshore systems experience wide-ranging and rapid temperature, salinity, and pH changes that may confound pH measurements when the response of both electrodes is combined. In principle, pHEXT can also be calculated via a half-cell reaction approach using the two half reactions specific to the Cl-ISE (reference electrode) and the ISFET (H $^+$ -sensitive measuring electrode). This approach effectively separates out and isolates the independent responses of the Cl-ISE to the activity of the chloride ion (Cl $^-$) (and salinity) and the ISFET to the activity of the hydrogen ion (H $^+$) (and pH).

To advance Sensor Best Practices for Durafet-based pH sensors, there

(mol (kg-H₂O)⁻¹), $E_{\rm EXT}$ replaces $E_{\rm cell}$ and is the measured sensor voltage, and $E_{\rm EXT}^*$ replaces $E_{\rm cell}^*$ and is the temperature-dependent calibration constant specific to the Cl-ISE that is related to the electrode standard potential ($E_{\rm EXT}^{\rm o}$) (Martz et al., 2010). S is the temperature-dependent Nernst slope and is calculated using Eq. (3).

$$S = \frac{RT}{F} \ln(10), \tag{3}$$

Here, R is the gas constant $(8.3145 \text{ J mol}^{-1} \text{ K}^{-1})$, T is temperature in Kelvin, and F is the Faraday constant $(96,485 \text{ C mol}^{-1})$ (Bard and Faulkner, 2001).

Ion activities are calculated using the empirical function for the mean activity coefficient of HCl $(\gamma_{\pm HCl} \text{ or } \gamma_H \gamma_{Cl})$ reported by Khoo et al. (1977) that is optimized for temperature and salinity between 5 and 40°C and 20 and 45, respectively. E_{EXT}^* is determined on the free scale in molality (mol (kg-H₂O) $^{-1}$). m_{Cl} is calculated from salinity following Dickson et al. (2007). Here, pH EXT is calculated as mol (kg-H₂O) $^{-1}$ assuming a 100% Nernst slope and a constant $dE_{EXT}^*/dT\text{emp}$ of -1.048 mV $^{^{0}}\text{C}^{-1}$ on the free scale from measured voltage, in situ temperature, and salinity. pH $^{EXT}_{free}$ in molality (mol (kg-H₂O) $^{-1}$) is converted to pH $^{EXT}_{total}$ in molinity (mol (kg-soln) $^{-1}$) during data processing. Please see section S1 in the Supplementary Materials for further discussion of these conversions. The complete cell reaction approach and its application are described in greater detail in Martz et al. (2010) and Bresnahan et al. (2014).

2.2. Half-cell (HC) reaction approach

2.2.1. Theory

 pH^{EXT} can be calculated via a half-cell (HC) reaction approach using the two half reactions specific to the chloride-sensitive CI-ISE that acts as the reference electrode (hereafter referred to as **REF**) and the H^+ -sensitive ISFET that acts as the working (or measuring) electrode (hereafter referred to as **work**). Based on the definitions provided in this section, pH^{EXT} will be shown to be on the total scale (pH^{EXT}_{total}). In the equations below, we follow the convention of Clegg and Whitfield (1991) in using κ_i to denote concentration in molinity or in terms of mol (kg-seawater (SW)) $^{-1}$ or mol (kg-soln) $^{-1}$.

The Cl-ISE half reaction is expressed by:

$$AgCl(s) + e^{-} \rightleftarrows Ag(s) + Cl^{-}, \tag{4}$$

where \mathbf{e}^- is an electron. The Cl-ISE half reaction has the following Nernst equation:

$$E_{REF} = E_{RFF}^{o} - Slog_{10}(^{\kappa}\gamma_{CI}\kappa_{CI}), \qquad (5)$$

where E_{REF} is the voltage, E_{REF}^{o} is the reference electrode standard potential that remains a function of temperature and pressure, κ_{Cl} is the total concentration of chloride in molinity or mol (kg-soln)⁻¹, and $\kappa_{Y_{Cl}}$ is the ion activity coefficient of chloride on a molinity basis (see section

Nernst equation for E_{EXT} (or E_{cell}) yields Eq. (9):

$$E_{\text{cell}} = E_{\text{EXT}} = E_{\text{REF}} - E_{\text{work.}} \tag{9}$$

Because the Cl-ISE responds to the chloride ion activity (Eq. (7)), E_{EXT} contains a chloride dependence as also noted by Bresnahan et al. (2014). The following Eqs. (10)–(20) show that the chloride activity dependence can be removed mathematically so that pH_{total}^{EXT} can be determined. Section 2.2.3 shows how to account for the chloride activity in a practical way. Eq. (9) can further be expanded into Eqs. (10) and (11).

$$E_{EXT} = E_{REF}^{o} - Slog_{10}(^{\kappa}\gamma_{CI}\kappa_{CI}) - (E_{work}^{o} + Slog_{10}(^{\kappa}\gamma_{H}\kappa_{H}))$$
(10)

$$E_{EXT} = E_{RFF}^{o} - E_{work}^{o} - Slog_{10}(^{\kappa}\gamma_{CI}\kappa_{CI}) - Slog_{10}(^{\kappa}\gamma_{H}\kappa_{H})$$
(11)

Eq. (11) is analogous to Eq. (1).

The electrode standard potential $(E_{cell}^o$ or E_{EXT}^o) is related to the standard potentials of the two half reactions and is defined in Eq. (12).

$$E_{\text{cell}}^{\text{o}} = E_{\text{EXT}}^{\text{o}} = E_{\text{REF}}^{\text{o}} - E_{\text{work}}^{\text{o}}, \tag{12}$$

 E_{REF}^{o} and E_{work}^{o} are defined in Eqs. (5) and (8), respectively. After substituting Eq. (12) for E_{EXT}^{o} into Eq. (11) and rearranging, pH^{EXT} is calculated from the two half reactions leading to Eq. (13), which is similar to Eq. (1a) using the complete cell reaction approach.

$$E_{EXT} = E_{EXT}^{o} - Slog_{10}(^{\kappa}\gamma_{H}^{\kappa}\gamma_{CI}\kappa_{CI}) - Slog_{10}(\kappa_{H}) = E_{EXT}^{o} - Slog_{10}(^{\kappa}\gamma_{H}^{\kappa}\gamma_{CI}\kappa_{CI}) + SpH^{EXT}$$

$$\tag{13}$$

2.2.3).

The H⁺-sensitive ISFET acts as an ion-selective electrode via hydrogen ion exchange represented by Eq. (6) between the overlying waters and the ISFET surface where >M represents the metal (*e.g.*, Al, Si, Ta, or Y) oxide at the surface of the ISFET electrode:

$$> M - OH + H3O+ \rightleftharpoons > M - OH2+ + H2O.$$
 (6)

Here, using half reactions, pH^{EXT} is calculated on the total scale $\left(pH_{total}^{EXT}\right)$ as concentration is in units of mol (kg-soln) $^{-1}$. Substituting Eq. (9) for E_{EXT} in Eq. (13) and rearranging to solve for pH^{EXT} yields Eq. (14):

$$pH_{total}^{EXT} = \frac{\left(E_{REF} - E_{work} - E_{EXT}^{o}\right) + Slog_{10}\left({}^{\kappa}\gamma_{H}{}^{\kappa}\gamma_{Cl}\kappa_{Cl}\right)}{S} = -log_{10}(\kappa_{H}). \tag{14}$$

Then, substituting Eq. (5) for E_{REF} into Eq. (14) yields Eq. (15):

$$pH_{total}^{EXT} = \frac{\left(E_{REF}^{o} - Slog_{10}\left({}^{\kappa}\gamma_{Cl}\kappa_{Cl}\right) - E_{work} - E_{EXT}^{o}\right) + Slog_{10}\left({}^{\kappa}\gamma_{H}{}^{\kappa}\gamma_{Cl}\kappa_{Cl}\right)}{S} = -log_{10}(\kappa_{H}). \tag{15}$$

For the measurement of the hydrogen ion (H⁺ and H_3O^+), the relationship between voltage, E, and ion activity, $\kappa_{a_{H^+}}$ (or κ_{a_H}) on the molinity scale (e.g., Bakker and Pretsch, 2007) is represented by Eq. (7):

$$E_{work} = E_{work}^{o} - Slog_{10}\left(\frac{1}{\kappa_{a_{H}}}\right) = E_{work}^{o} + Slog_{10}(\kappa_{a_{H}}), \tag{7}$$

where E_{work} is the voltage measured by the working electrode and E_{work}^0 is the working electrode standard potential that remains a function of temperature and pressure. Eq. (7) can be further expanded into Eq. (8):

$$E_{work} = E_{work}^{o} + S \log_{10}(^{\kappa}\gamma_{H}\kappa_{H}), \tag{8}$$

where $^{\kappa}\gamma_{H}$ is the ion activity coefficient of hydrogen on a molinity basis and κ_{H} is the total hydrogen ion concentration in terms of mol (kg-soln) $^{-1}$.

The sum of the half reaction from Eq. (4) and the reverse of the half reaction from Eq. (6) yields the complete cell potential equation (e.g., Eq. (1)) as shown in the following derivation. When combining the Nernst equations for the half reactions from Eqs. (5) and (8), the full

Eq. (15) can further be simplified by removing redundant $\log_{10}({}^{\kappa}\gamma_{CI}\kappa_{CI})$ terms which leads to Eq. (16) and the removal of chloride activity or dependence for pH^{EXT}_{total}:

$$pH_{total}^{EXT} = \frac{\left(E_{REF}^{o} - E_{work} - E_{EXT}^{o}\right) + Slog_{10}\left(^{\kappa}\gamma_{H}\right)}{S}. \tag{16}$$

 pH_{total}^{EXT} calculation still utilizes a conventional electrode standard potential $\left(E_{EXT}^{o}\right)$ (as seen in Eqs. (12) and (16)) while the equivalent parameter in Eq. (2) for pH_{free}^{EXT} calculation is referred to as a calibration constant denoted by an asterisk $\left(E_{EXT}^{\circ}\right)$ rather than a nought symbol $\left(E_{EXT}^{o}\right)$ (Martz et al., 2010). Therefore, for calibration purposes, we relate E_{EXT}^{o} to a new calibration constant term, $E_{EXT,he}^{*}$, which is defined in Eq. (17) and contains the activity coefficient of the hydrogen ion, $^{\kappa}\gamma_{H}$:

$$E_{EXT,bc}^* = E_{EXT}^o - Slog_{10}(^{\kappa}\gamma_H). \tag{17}$$

Eq. (17) can be rearranged to Eq. (18) to solve for E_{EXT}^{o} :

$$E_{\text{EXT}}^{\text{o}} = E_{\text{EXT,hc}}^{*} + \text{Slog}_{10}(^{\kappa}\gamma_{\text{H}}). \tag{18}$$

After substituting Eq. (18) for E_{EXT}^0 back into Eq. (16), Eq. (19) results:

$$pH_{total}^{EXT} = \frac{\left(E_{REF}^{o} - E_{work} - \left(E_{EXT,hc}^{*} + Slog_{10}\left(^{\kappa}\gamma_{H}\right)\right)\right) + Slog_{10}\left(^{\kappa}\gamma_{H}\right)}{S}. \tag{19}$$

Eq. (19) can further be simplified by removing the redundant $S \log_{10}(\kappa \gamma_H)$ term to produce the final equation for calculating pH^{EXT}:

$$pH_{total}^{EXT} = \frac{\left(E_{REF}^{o} - E_{work} - E_{EXT,hc}^{*}\right)}{S}.$$
 (20)

In this form, pH^{EXT} is directly calculated on the total scale (pH^{EXT}_{total}) from the calibration constant, $E^*_{EXT,hc}$. In turn, $E^*_{EXT,hc}$ can be calculated from pH^{EXT}_{total} using a rearranged version of Eq. (20) (shown in Eq. (21)):

$$E_{\text{EXT.hc}}^* = E_{\text{REF}}^{\text{o}} - E_{\text{work}} - S \, pH_{\text{total}}^{\text{EXT}}. \tag{21}$$

Lastly, $E_{EXT,hc}^*$ can also be calculated from pH_{free} using Eq. (22) via:

$$E_{EXT,hc}^{*} = \left(E_{REF}^{o} - E_{work} - S pH_{free}^{EXT}\right) + S \log_{10} \left(1 + \frac{\left[SO_{4}^{2-}\right]_{total}}{K_{S}}\right), \tag{22}$$

where $\left[SO_4^{2-} \right]_{total}$ and K_S are the total sulfate concentration and the bisulfate $\left(HSO_4^{2-} \right)$ dissociation constant, respectively. Equations for $\left[SO_4^{2-} \right]_{total}$ and K_S are included in Dickson et al. (2007). $E_{EXT,hc}^*$ can be evaluated from primary pH standards (e.g., TRIS buffer) or pH_{total} determined from discrete samples measured using established benchtop spectrophotometric methods that are calibrated to and developed using TRIS buffers. By utilizing single ion activity coefficients (e.g., $^{\kappa}\gamma_H$ and $^{\kappa}\gamma_{CI}$), the half-cell reaction approach enables calculation of pH $_{total}^{EXT}$ directly without the need to perform the calibration on the free scale.

2.2.2. Application

pH_{total} is now calculated using Eq. (20) via the following steps:

a) E_{REF}° is calculated from the standard potential equation for the Ag/AgCl reference electrode from Bates and Bower (1954) valid over a range of temperatures between 0° and 90 °C:

c) The ion activity coefficient of chloride ($^{\kappa}\gamma_{Cl}$) for each discrete sample and sensor measurement is calculated according to the Davies convention summarized in Stumm and Morgan (1996):

$$log_{10}\big(^{\kappa}\gamma_{Cl}\big) = -Az^2\Big(\frac{I^{1/2}}{1+I^{1/2}} - 0.2I\Big), \tag{25} \label{eq:25}$$

where A is the Debye-Hückel constant (in units of (kg-soln)^{1/2} mol^{-1/2}), z is the charge of the chloride ion, and I is the ionic strength which is proportional to salinity where I = 0.697 mol (kg-soln)⁻¹ at a salinity of 35. In this work, ${}^{\kappa}\gamma_{CI}$ on a molinity basis is optimized for up to $I \leq 0.7$ (please see section 5.5 and section S2 in the Supplementary Materials for further discussion). The Debye-Hückel constant, A, for each discrete sample and sensor measurement, is calculated using Eq. (26):

$$A = \frac{1}{2.303} (2\pi N_{\rm A} \rho)^{1/2} \left(\frac{e^2}{4\pi\epsilon_0 \epsilon k_B T}\right)^{3/2}, \tag{26}$$

where N_A is Avogadro's number $(6.022\times10^{23}~mol^{-1}), \rho$ is the density in kg-soln m^{-3} , e is the charge of an electron $(1.602\times10^{-19}~C), \epsilon_0$ is the permittivity of free space $(8.8540\times10^{-12}~C^2~N^{-1}~m^{-2}~or~C^2~J^{-1}~m^{-1}), \epsilon$ is the dielectric constant of seawater, k_B is the Boltzmann Constant $(1.3807\times10^{-23}~J~K^{-1}),$ and T is the temperature in Kelvin (Alberty and Daniels, 1979). ρ in units of kg-soln m^{-3} at 1 atm is calculated from coincident temperature and salinity measured by the integrated SBE37 temperature-conductivity sensor following the equations of Millero and Poisson (1981). ϵ is calculated from the same coincident sensor-measured temperature and salinity using the equations from Klein and Swift (1977). For a complete description of the equations used to calculate ρ and ϵ , please see section S2 in the Supplementary Materials.

d) To calculate E_{work} , E_{REF} is first calculated using Eq. (5) from parameters calculated in Eqs. (23)–(25). In turn, E_{work} is calculated from E_{REF} and E_{EXT} measured by the sensor using an expanded version (Eq. (9a)) of Eq. (9):

$$E_{work} = E_{REF} - E_{EXT} = E_{REF}^{o} - Slog_{10}(^{\kappa}\gamma_{CI} \kappa_{CI}) - E_{EXT}. \tag{9a}$$

As E_{EXT} still contains a chloride ion activity dependence from the term — $Slog_{10}(^{\kappa}\gamma_{CI}\kappa_{CI})$ (see Eq. (11)), this procedure mathematically removes the activity by calculating its activity coefficient (Eq. (25)) and ac-

$$E^{0}(V) = E_{RFF}^{0} = 0.23659 - (4.8564 \times 10^{-4})t - (3.4205 \times 10^{-6})t^{2} + (5.869 \times 10^{-9})t^{3},$$
(23)

where t is temperature in degrees Celsius. Bates and Bower (1954) reported an average deviation of 0.04 mV from Eq. (23) and their experimental values (n = 16).

b) The chloride ion concentration (κ_{Cl}) in mol kg-soln⁻¹ at another salinity is calculated from the corresponding salinity measurement assuming the constant seawater κ_{Cl} /Salinity ratio of 0.5458696 mol (kg-soln)⁻¹ at a salinity of 35 from Millero et al. (2008) via Eq. (24):

counting for the concentration of chloride determined from the salinity data (Eq. (24)).

e) The Nernst slope is calculated using Eq. (3) from in situ temperature (e.g., temperature measured by the integrated SBE37 temperatureconductivity sensor on a SeapHOx sensor or another co-located sensor).

$$\kappa_{C1} \left(\text{mol} \left(kg - \text{soln} \right)^{-1} \right) = \text{Salinity} \left(kg - \text{soln} \right)^{-1} x \left(\frac{0.5458696 \text{ mol} \left(kg - \text{soln} \right)^{-1}}{35 \left(kg - \text{soln} \right)^{-1}} \right). \tag{24}$$

f) $E_{EXT,hc}^*$ at *in situ* temperature ($E_{EXT,hc}^*(t)$) is calculated using Eq. (21) from E_{REF}^o , E_{work} , and the reference pH on the total scale corrected to

in situ temperature (e.g., pH_{total} of discrete samples used to validate sensor performance corrected to in situ temperature, pH_{total}^{disc}). Thus, pH_{total}^{disc} substitutes for pH_{total}^{EXT} in Eq. (21).

- g) Since $E^*_{EXT,hc}$ is a function of temperature, an independent $dE^*_{EXT,hc}/dT$ emp must be constrained to correct data to a reference temperature as is recommended by current Sensor Best Practices (Bresnahan et al., 2014). Values of $E^*_{EXT,hc}$ at in situ temperature ($E^*_{EXT,hc}(t)$) calculated from pH $^{disc}_{total}$ are regressed against in situ temperature measured by the SBE37 conductivity-temperature sensors integrated with SP033 and SP053. Slopes of these regressions are used as experimental $dE^*_{EXT,hc}/dT$ emp for each sensor. For more details, please see section S3 in the Supplementary Materials.
- h) Values of $E^*_{EXT,hc}(t)$ are corrected to a reference temperature of 25°C ($E^*_{EXT,hc,25}$) using experimental $dE^*_{EXT,hc}/dT$ emp using Eq. S14 in section S3 of the Supplementary Materials. A reference temperature of 25°C is used since this was the original reference temperature used for the nomenclature for SP033 and SP053 described in Bresnahan et al. (2014). For more details, please see section S3 in the Supplementary Materials.
- Calculate and apply a single value of E*_{EXT,hc,25} to calibrate the raw sensor-measured pH timeseries; please see section 4.3 for further discussion of the sensor calibration.
- j) Calculate the final calibrated pH at in situ temperature using the desired value of E^{*}_{EXT,hc,25} using Eq. S15 in section S3 of the Supplementary Materials. Please see this section for more details.

A flow chart that summarizes how to determine parameters used in the half-cell reaction approach is included in Appendix 1.

3. Materials

3.1. Test tanks

Two 1268-liter rectangular fiberglass tanks (L x W x H = $0.914 \times$ 0.914×1.524 m) were requisitioned and used for this work (hereafter referred to as Tank 1 and Tank 2). The tanks were housed in the Smith Laboratory Greenhouse on the University of Delaware's Hugh R. Sharp Campus (Lewes, DE, USA). Tank 1 was equipped with continuous duty Danner Mfg. Supreme Aqua-Mag Magnetic Drive Model 5 and Model 7 submersible pumps which were capable of mixing water at a combined rate of >4500 liters per hour (LPH) to keep its waters well-mixed. Tank 2 was equipped with a single continuous duty Model 7 submersible pump (2650 LPH) for the same purpose. Salinity was decreased and increased using deionized (DI) water and seawater (SW), respectively, provided by the University of Delaware from a coastal site (salinity 30.86). Tank 2 was used to house the lowest salinity treatment. In Tank 2, DI water and seawater were mixed in an appropriate ratio to produce a final salinity of \sim 1.3–1.4 and DI water was added as needed to maintain an approximate 0.775-m water level to counter evaporation over time.

3.2. Instrumentation

To take advantage of sensor redundancy, two SeapHOx sensors, SP033 and SP053, were used in this work. The SeapHOx sensor package includes sensors for pH (Honeywell Durafet), dissolved oxygen (Aanderaa Data Instruments 4835 Optode), and temperature and salinity (reported on the Practical Salinity Scale, PSS-78) (Sea-Bird Electronics Conductivity-Temperature Sensor – SBE37), plumbed into a continuous flow path that is flushed by a Sea-Bird Electronics (SBE) 5M submersible pump (Bresnahan et al., 2014). SP033 and SP053 were equipped and programmed identically with 30-min sampling intervals, 65-sec pump times, and 20-pH sample averages (equivalent to 16-sec measurement periods). Pump times were systematically increased to facilitate a

complete flushing of the flow housing over individual sampling cycles as salinity and pH changed. The SeapHOx sensors utilize off-the-shelf Orion Cl-ISEs.

The Cl-ISE in SP033 was replaced in February 2022 after leakage around the seal of the outer perimeter of the AgCl pellet was observed, and it was then stored in seawater inside the sensor flow housing prior to sensor pre-conditioning in seawater in Tank 1 in May 2022. SP053 was removed from Tank 1 and its Cl-ISE was also replaced on 1 June 2022 for the same reason. Visual inspection of the Cl-ISE surfaces before and after the tank tests indicated no abrasion, discoloration, or leakage. SP033 and SP053 were deployed vertically and upright in the tanks and were also bolted together to prevent them from falling over to one side due to the weight of their SBE37 conductivity-temperature sensors. The sensors and test tank setup are shown in Fig. S4 in the Supplementary Materials.

4. Procedures

4.1. Salinity cycling

SP033 and SP053 were subject to salinity, and by extension, pH decreases and increases between 1 and 31 and 6.9 and 8.1, respectively. over a six-day period between 12 June 2022 and 17 June 2022. The tank tests were designed to simulate the range of environmental conditions observed during tidal mixing in the Murderkill Estuary-Delaware Bay System (Bowers, DE, USA) (described by Gonski et al. (2018, 2023) and Pettay et al. (2020)). Under this design, a single salinity change was simulated via dilution using DI water or concentration using seawater between the 30-min sampling intervals of the sensor; afterwards the sensors were allowed to equilibrate and respond to the new environmental conditions for ~24 h. Prior to beginning the salinity (and pH) cycling experiments, SP033 and SP053 underwent continuous conditioning using a 4 h sampling interval in Tank 1 in seawater (salinity between 30 and 33) between 15 May 2022 and 12 June 2022. The salinity cycling experiments are described in greater detail in section S4 of the Supplementary Materials.

4.2. Discrete sampling approach

To monitor and validate the sensor responses of SP033 and SP053, discrete water samples were collected from the tanks over the first six hours following salinity dilution and concentration on Days 1–3 and Days 4–6, respectively, coincident with sensor measurements. To conserve water in the tanks and reduce sampling times, discrete water samples were collected unfiltered. Separate samples for total alkalinity (TA) and pH_{total} were collected using a submersible pump positioned at the approximate defined depth of the SeapHOx intake by bottom-filling into triple-rinsed 250-mL borosilicate glass bottles. During sample collection, samples were overflowed for at least once their volume to minimize contact with the atmosphere. After collection, samples were poisoned with 50 μ L of saturated mercuric chloride solution (HgCl₂) and stored in the dark at \sim 4°C and were analyzed within five days of collection. Salinity was also measured independently on each TA and pH_{total} sample.

Discrete water samples were collected ahead of each salinity step to approximate the initial condition and then every 30 min between Hours 0 and 3 and every 60 min between Hours 4 and 6. On Days 1–2 and 5–6, duplicate samples were collected when collecting initial condition samples and then during Hours 2, 4, and 6. On Days 3 and 4, when sensors were moved between tanks, duplicate samples were collected when collecting initial condition samples and then during Hours 0, 2, 4, and 6. Hour 0 corresponds to the first sensor measurements after salinity fully changed due to dilution or concentration during all six days. Further discrete water samples were also collected at 22:30 on 18 June 2022 and 15:00 on 19 June 2022 during the post-cycling period. This sampling design yielded a total of 94 discrete waters for sensor validation. The analytical methods used to measure TA, spectrophotometric

pH_{total}, and salinity (on the Practical Salinity Scale) of the discrete water samples are described in section S5 of the Supplementary Materials.

4.3. Sensor calibration

With 94 discrete samples for pH_{total} collected over 68 different sampling points, a multi-point in situ or field calibration was used for SP033 and SP053 (Bresnahan et al., 2014; Gonski et al., 2018; Miller et al., 2018). Discrete sample in situ pHtotal values (pHtotal) were derived using the MATLAB version of CO2SYS (v3.2.0; Sharp et al., 2020) with input parameters of salinity, in situ temperature (from the integrated SBE37 sensors), pH_{total}, and TA using the carbonic acid dissociation constants of Millero et al. (2006), the bisulfate dissociation constant of Dickson (1990), and total boron from Uppström (1974). To calibrate SP033 and SP053, the discrete samples collected during the six-hour period after the salinity steps were used as calibration samples (n =78) whereas the initial condition samples and post-cycling period discrete samples were used as reference samples (n = 12) to check and validate the calibration at the same salinity step. After quality control of the pH_{total} data, four discrete samples were identified as outliers. These four discrete samples included - (a) one duplicate sample collected at Hour 6 on Day 3, (b) two initial condition samples collected before salinity was increased on Day 4, and (c) one sample collected at Hour 5 on Day 4. These four discrete samples were removed and omitted from further analyses.

Based on the results of this work, we employed two different iterations of the multi-point $in\ situ$ or field calibration. First, as dictated by Sensor Best Practices, average values of $E_{EXT,hc}^*$ and E_{EXT}^* for the half-cell and complete cell reaction approaches, respectively, were calculated based on all valid calibration samples and retroactively applied to raw pH sensor timeseries to minimize the anomaly between the sensor pH and the discrete sample pH (Bresnahan et al., 2014). Second, we propose splitting $E_{EXT,hc}^*$ and E_{EXT}^* as necessary depending on the direction of salinity change and/or ending salinity when distinct and stable values of $E_{EXT,hc}^*$ and E_{EXT}^* are reached over single or multiple days (discussed

further in section 5.2). To do this, $E_{EXT,hc}^*$ and E_{EXT}^* were split out and then average values were calculated using the corresponding subset of calibration samples. Afterwards, the average $E_{EXT,hc}^*$ and E_{EXT}^* were applied independently to each segment of the raw pH sensor timeseries to calculate the final pH $_{\text{total}}^{EXT}$. The segments were then recombined to restore a continuous timeseries.

Model II least squares fits of pH_{total}^{disc} and pH_{total}^{EXT} (Peltzer, 2007) for selected full pH_{total} timeseries were performed to generate sensor gains (or slopes, c_1) and sensor offsets (or intercepts, c_0). Finally, root-mean square errors (RMSE) of their fits were calculated. To distinguish between the different pH_{total}^{EXT} timeseries, pH_{total}^{EXT} calculated using the complete cell reaction approach will hereafter be referred to as $pH_{total,single}^{EXT,CC}$ and $pH^{EXT,CC}_{total,split}$ when timeseries are recalibrated using a single E^{\ast}_{EXT} and when E_{EXT}^* are split out before recalibration, respectively. Similarly, pH_{total} calculated using the half-cell reaction approach will hereafter be referred to as $pH_{total,single}^{EXT,HC}$ and $pH_{total,split}^{EXT,HC}$ using the same criteria. For discussion of the accompanying pH uncertainty propagation for the discrete samples using the equations from Khalsa et al. (2021), please see section S6 in the Supplementary Materials. Finally, weather- and climate-level pH data quality thresholds established by the Global Ocean Acidification Observation Network (GOA-ON) (Newton et al., 2015) were used as ocean acidification (OA) community-standard pH data quality thresholds to provide further context for our results; these correspond to ± 0.02 and ± 0.003 pH, respectively.

5. Results and discussion

5.1. Tank test conditions

The test tanks remained open to the ambient atmosphere for the duration of the work. Ambient water temperature (Fig. 1a) followed atmospheric temperature and varied between 21 and 32°C. Water temperature exhibited diel variability between day and night with the

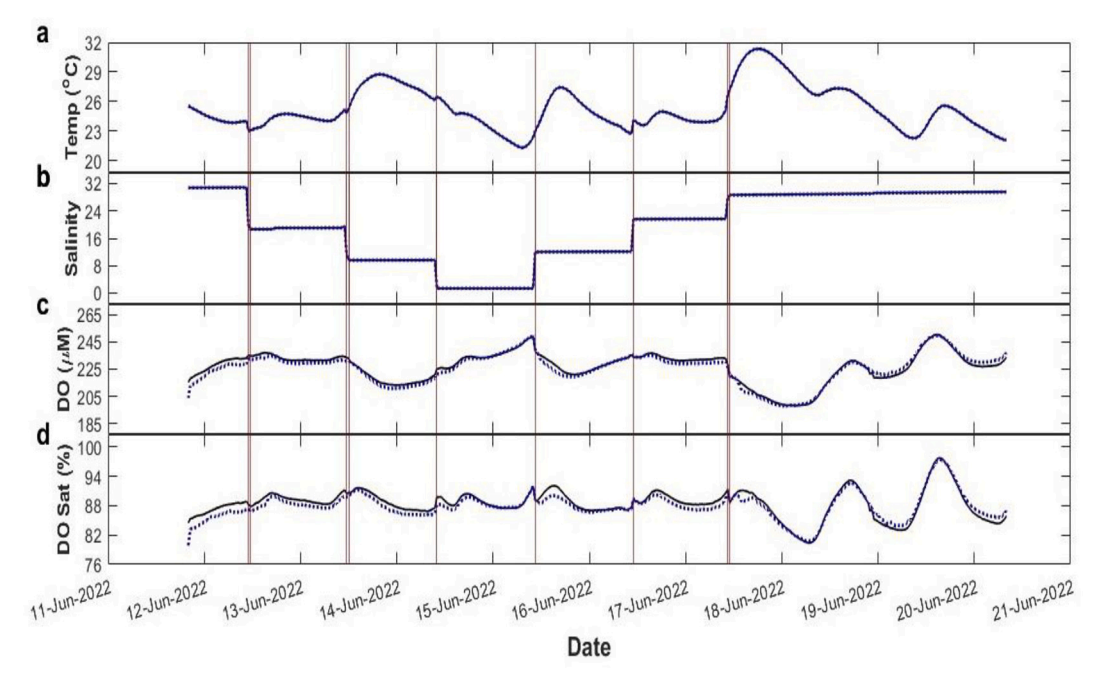


Fig. 1. Tank test time-series between 11 June 2022 and 21 June 2022. Panels (a) and (b) show in situ temperature and salinity, respectively, measured by the integrated SBE37 temperature-conductivity sensors on SP033 (solid black) and SP053 (dotted blue). Panels (c) and (d) show dissolved oxygen (DO) and dissolved oxygen saturation (DO sat), respectively, measured by the integrated Aanderaa 4835 optodes on SP033 (solid black) and SP053 (dotted blue). Vertical red lines denote the first sensor measurements after salinity cycling. (For interpretation of the references to color in this figure legend, the reader is referred to the web version of this article.)

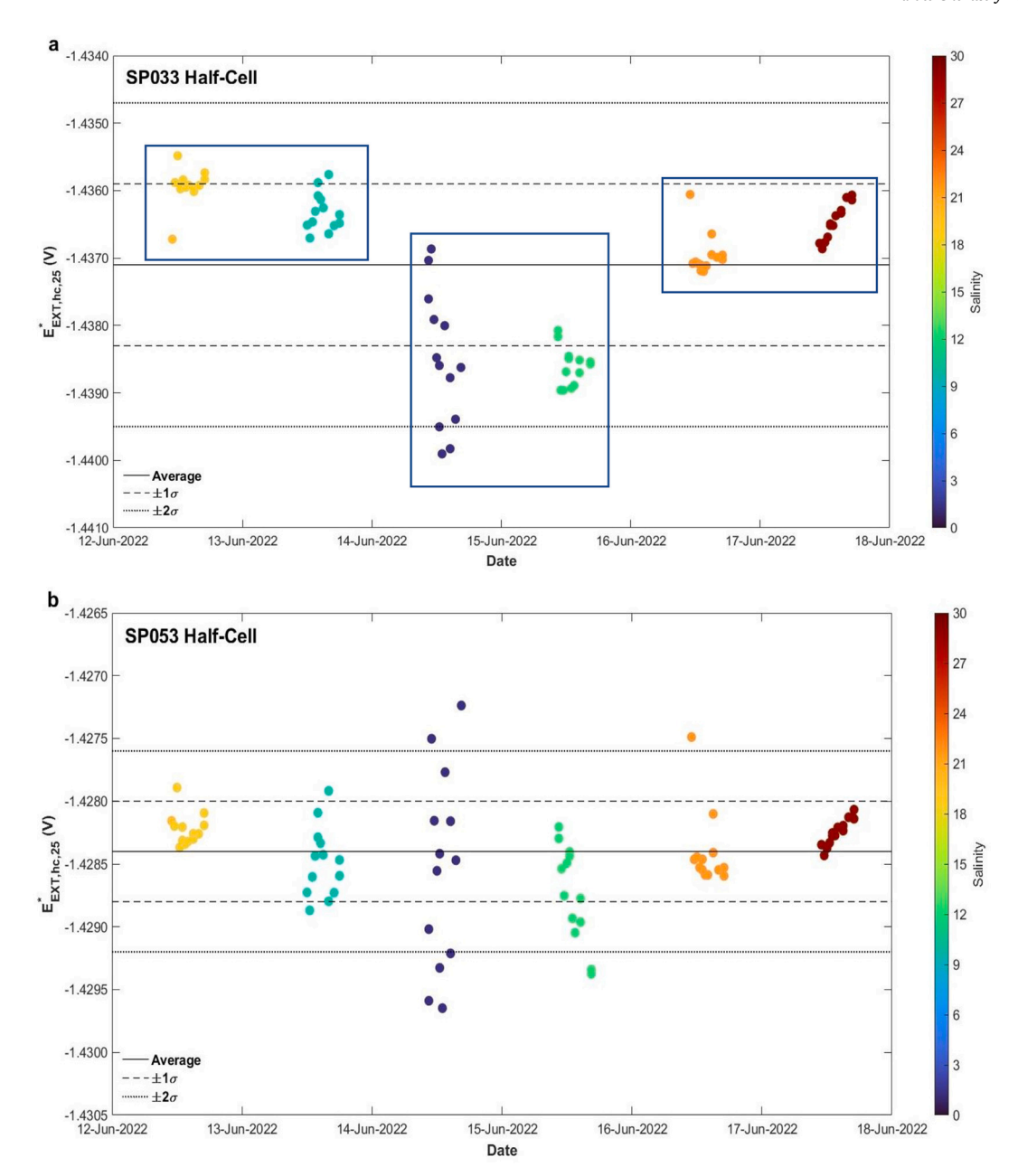


Fig. 2. Timeseries of $E^*_{EXT,hc}$ corrected to a reference temperature of 25°C $\left(E^*_{EXT,hc,25}\right)$ using experimental $dE^*_{EXT,hc}/dT$ emp for (a) SP033 and (b) SP053 as a function of salinity (color-coded) relative to their average values (solid black lines) and ± 1 (dashed black lines) and ± 2 (dotted black lines) standard deviations. $E^*_{EXT,hc,25}$ is calculated on the total scale. Raw data measured with SP033 were split between Days 1–2, Days 3–4, and Days 5–6 for recalibration (indicated by blue boxes in panel (a)). (For interpretation of the references to color in this figure legend, the reader is referred to the web version of this article.)

warmest temperatures in the late afternoon and the early evening and the coolest temperatures late at night and in the early morning. Diel temperature variability gives this evaluation and calibration procedure similarity to in situ field sensor deployments. Salinity (Fig. 1b) was diluted on Days 1–3 and concentrated on Days 4–6 as reflected in the stairstep profile of the salinity data. For further discussion of the temperature and salinity data, please see section S7, Table S3, and Figs. S5-S7 in the Supplementary Materials. Dissolved oxygen (DO) (Fig. 1c) and DO percent saturation (Fig. 1d) varied between 197 and 251 $\mu\rm M$ and 79% and 98%, respectively, across both sensors.

5.2. Treatment of calibration constants

5.2.1. In situ temperature

 $E^*_{\rm EXT,hc}(t)$ (calculated on total scale) and $in\,situ$ temperature (Table S1 and Fig. S3a-b) did not always conform to a single defined relationship (or linear function). Plots of $E^*_{\rm EXT,hc}(t)$ and $in\,situ$ temperature for SP033 (Fig. S3a) revealed three distinct relationships that were isolated to single or pairs of specific days from the tank tests that nominally aligned with the direction of salinity change and/or ending salinity values for Days 1–2, Day 3–4, and Days 5–6. Day 3 data collected at salinities 1.38–1.41 broadly aligned with Day 4 but Day 3 data were scattered around the more linear Day 4 data. In contrast, $E^*_{\rm EXT,hc}(t)$ and $in\,situ$ temperature for SP053 (Fig. S3b) produced a single distinct relationship over all temperatures and salinities. However, like SP033, data from Day

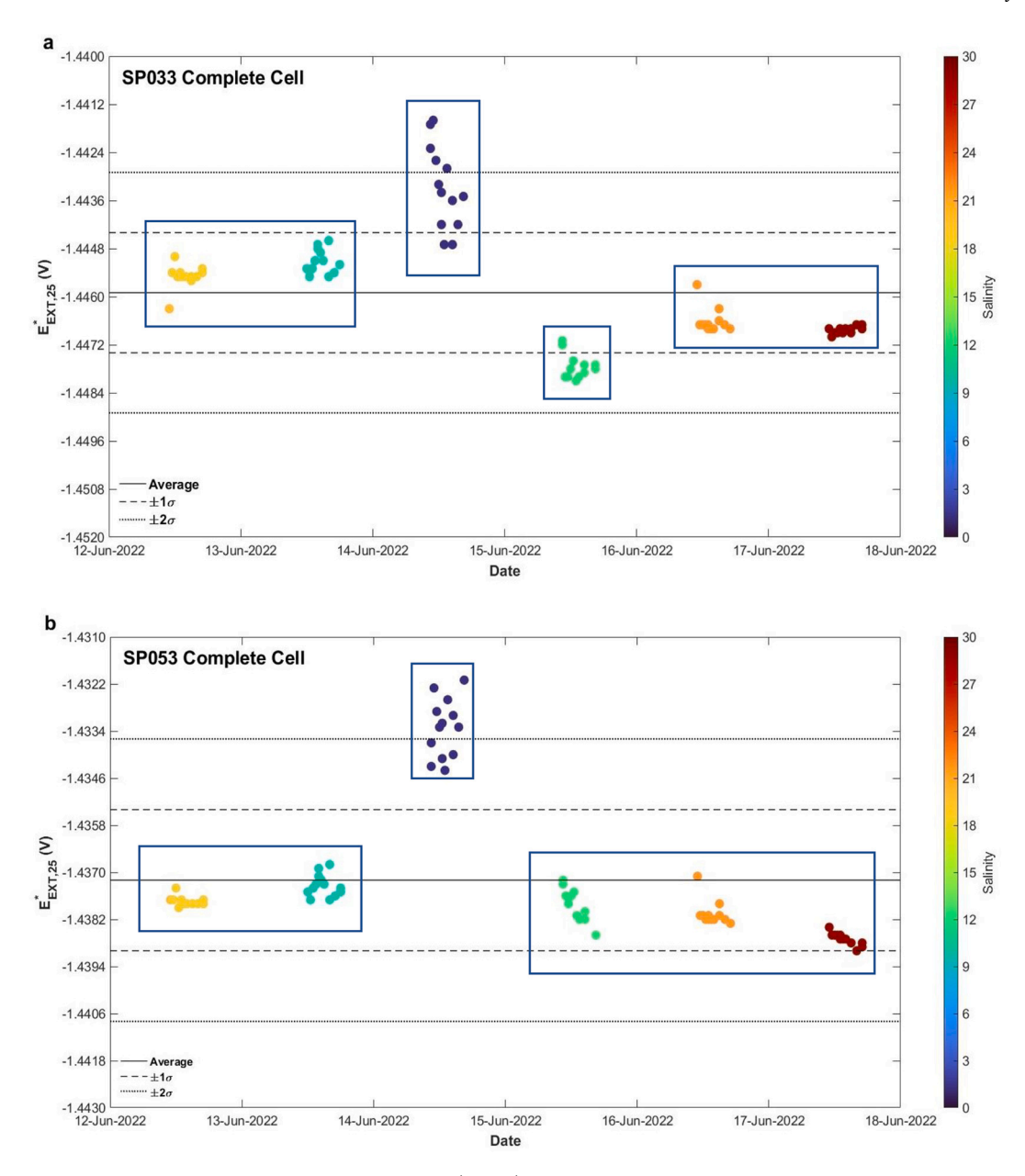


Fig. 3. Timeseries of E_{EXT}^* corrected to a reference temperature of $25^{\circ}C$ ($E_{EXT,25}^*$) using dE_{EXT}^*/dT emp from Martz et al. (2010) for (a) SP033 and (b) SP053 as a function of salinity (color-coded) relative to their average values (solid black lines) and ± 1 (dashed black lines) and ± 2 (dotted black lines) standard deviations. $E_{EXT,25}^*$ is calculated on the free scale. Raw data measured with SP033 were split between Days 1-2, Day 3, Day 4, and Days 5-6 for recalibration (indicated by blue boxes in panel (a)). Raw data measured with SP053 were split between Days 1-2, Day 3, and Days 4-6 for recalibration (indicated by blue boxes in panel (b)). (For interpretation of the references to color in this figure legend, the reader is referred to the web version of this article.)

3 at salinities 1.38–1.41 exhibited more scatter. Slopes of relationships between $E^*_{EXT,hc}(t)$ and in~situ temperature were used as experimental $dE^*_{EXT,hc}/dT$ emp for each sensor as defined in section 2.2.2. Please see section S3 of the Supplementary Materials for further discussion of the role and determination of $dE^*_{EXT,hc}/dT$ emp.

Values of E_{EXT}^* (calculated on the free scale) were corrected back to in situ temperature ($E_{EXT}^*(t)$) from their reference temperature of 25°C (as discussed in Bresnahan et al. (2014)) and scrutinized for similar behavior. Plots of $E_{EXT}^*(t)$ and in situ temperature for SP033 and SP053 (Table S4 and Fig. S8) revealed that $E_{EXT}^*(t)$ exhibited a similar behavior. For SP033 (Fig. S8a), $E_{EXT}^*(t)$ and in situ temperature exhibited four distinct relationships or clusters that nominally aligned to the direction of salinity change and/or ending salinity value for Days 1–2, Day 3, Day

4, and Day 5–6. For SP053 (Fig. S8b) $E_{EXT}^*(t)$ and $in\ situ$ temperature exhibited three distinct relationships or clusters for Days 1–2, Day 3, and Days 4–6. Day 3 data exhibited more scatter at salinities 1.38–1.41. Moreover, calculating $E_{EXT}^*(t)$ on the free scale causes a positive shift in the Day 3 $E_{EXT}^*(t)$ data at salinities 1.38–1.41 relative to the $E_{EXT}^*(t)$ data for Days 1–2 and 4–6 at salinity >9.6–9.7, as expected due to the $\left[SO_4^{2-1}\right]_{total}$ change. This behavior is not seen with $E_{EXT,hc}^*(t)$ that is calculated on the total scale. Please see section S8 of the Supplementary Materials for further discussion of the treatment of values of $E_{EXT}^*(t)$.

5.2.2. Reference temperature: 25°C

At the reference temperature of 25°C, $E^*_{EXT,hc,25}$ (calculated on the total scale; Fig. 2 and Table S5 in the Supplementary Materials) and

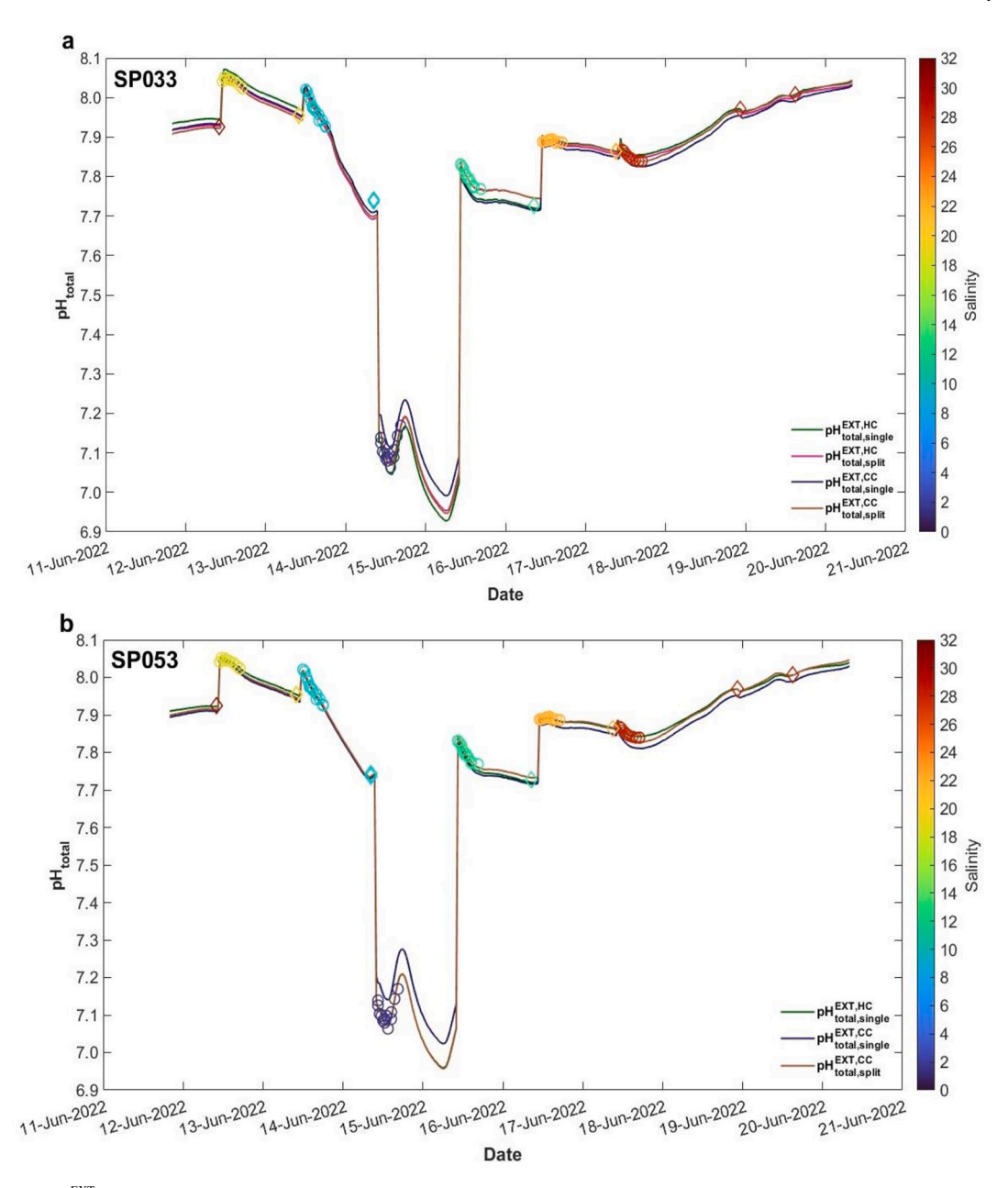


Fig. 4. Tank test sensor pH_{total} time-series between 11 June 2022 and 21 June 2022 for (a) SP033 and (b) SP053 shown relative to pH_{total} of calibration samples (open circles) and reference samples (open diamonds) as a function of salinity (color-coded). Timeseries of pH_{total,single} (dark green), pH_{total,split} (dark pink), pH_{total,single} (dark blue), and pH_{total,split} (sienna) are shown. In panel (a) for SP033, pH_{total,split} (dark pink) and pH_{total,split} (sienna) largely overlap. (For interpretation of the references to color in this figure legend, the reader is referred to the web version of this article.)

 $E_{\rm EXT,25}^*$ (calculated on the free scale; Fig. 3 and Table S5 in the Supplementary Materials) between Days 1 and 6 of the tank tests match the behavior exhibited by relationships between $E_{\rm EXT,hc}^*(t)$ or $E_{\rm EXT}^*(t)$ and in situ temperature for each sensor for the half-cell and complete cell reaction approaches, respectively. For SP033, three visually distinct clusters of $E_{\rm EXT,hc,25}^*$ (Fig. 2a) were observed over Days 1–2, 3–4, and 5–6 using the half-cell reaction approach while four visually distinct clusters of $E_{\rm EXT,25}^*$ (Fig. 3a) were observed over Days 1–2, 3, 4, and 5–6 for the complete cell reaction approach. On the other hand, for SP053, $E_{\rm EXT,hc,25}^*$ (Fig. 2b) remained constant and stable over all six days for the half-cell reaction approach whereas three visually distinct clusters of $E_{\rm EXT,25}^*$ (Fig. 3b) were observed over Days 1–2, 3, and 4–6. Therefore, $E_{\rm EXT,hc,25}^*$ and $E_{\rm EXT,25}^*$ were split and grouped thusly based on the distinct clusters

observed for each sensor. Average values of $E^*_{EXT,hc,25}$ or $E^*_{EXT,25}$ were then calculated using the subset of calibration samples and applied independently to the segment of sensor data specific to each cluster of $E^*_{EXT,hc,25}$ or $E^*_{EXT,25}$. Average values of $E^*_{EXT,hc,25}$ and $E^*_{EXT,25}$ that were used to recalibrate the raw sensor data for both sensor calibration methods are given in Table S6 in section S9 of the Supplementary Materials.

5.3. Bottle sample and sensor pH comparisons

Over the course of the tank tests, pH_{total}^{disc} and salinity of the discrete samples (Fig. 4) varied between 7.06 and 8.06 and 1 and 31, respectively. On Day 1, pH_{total}^{disc} in Tank 1 increased from 7.92 to 8.04 when salinity was diluted from 30.86 to 18.66 and it remained relatively

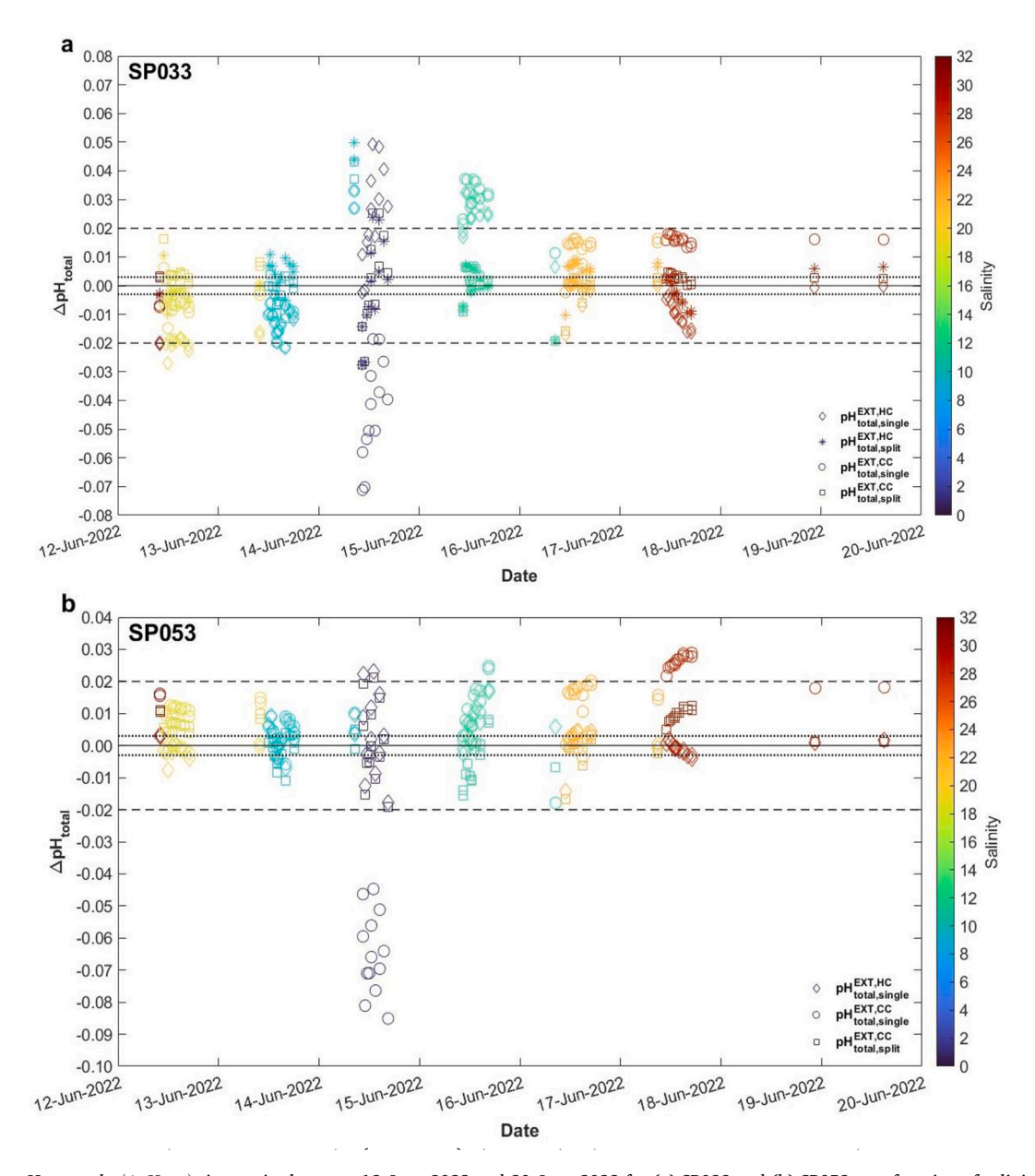


Fig. 5. Tank test pH anomaly (ΔpH_{total}) time-series between 12 June 2022 and 20 June 2022 for (a) SP033 and (b) SP053 as a function of salinity (color-coded). Values of ΔpH_{total} are shown relative a zero anomaly (solid black line) and GOA-ON weather-level $(\pm 0.02 \text{ pH}; \text{ dashed black lines})$ and climate-level $(\pm 0.003 \text{ pH}; \text{ dotted black lines})$ pH data quality thresholds. Values of ΔpH_{total} between pH_{total}^{disc} and $pH_{total,single}^{EXT,HC}$ (open diamonds), $pH_{total,split}^{EXT,HC}$ (asterisks), $pH_{total,single}^{EXT,CC}$ (open squares) are shown. Reference samples are the samples of a different salinity that precede clusters of calibration samples and the single samples from 18 and 19 June 2022.

stable between 8.02 and 8.06 over the course of the six-hour sampling period. On Day 2, pH_{total}^{disc} in Tank 1 increased slightly from 7.95 to 8.02 when salinity was diluted from 19.66 to 9.60, and then, further decreased to 7.92 over the six-hour sampling. Between Days 2 and 3, pH_{total}^{disc} decreased by $\sim\!0.2$ to 7.74. When the sensors were switched between test tanks on Day 3, pH_{total}^{disc} and salinity decreased from 7.74 and 9.66 in Tank 1 to 7.13 and 1.38, respectively, in Tank 2. Over the six-hour sampling period on Day 3, pH_{total}^{disc} varied between 7.06 and 7.17.

When concentrating salinity on Day 4 by switching the sensors back to Tank 1, pH $_{\rm total}^{\rm disc}$ and salinity increased to 7.83 and 12.05, respectively, pH $_{\rm total}^{\rm disc}$ then slowly decreased to 7.75 over the six-hour sampling period on Day 4. When concentrating salinity further on Day 5 in Tank 1 by adding seawater with salinity and pH $_{\rm total}$ of 30.86 and 7.88, respectively, pH $_{\rm total}^{\rm disc}$ and salinity increased from 7.73 and 12.13 to 7.89 and 21.60,

respectively. pH $_{total}^{disc}$ remained stable between 7.88 and 7.90 over the six-hour sampling period on Day 5. On Day 6, pH $_{total}^{disc}$ only changed marginally from 7.86 to 7.87 while salinity increased from 21.68 to 28.65 when adding seawater with salinity and pH $_{total}$ of 30.86 and 7.94, respectively, in Tank 1. Over the post-cycling period, pH $_{total}$ and salinity further increased to >8.0 and > 29.5, respectively, prior to sensor recovery. The propagated uncertainty (Q) for all calibration and reference samples (discussed in section S6 and shown in Table S2 of the Supplementary Materials) was better than \leq 0.0072 pH.

Throughout the salinity (and pH) cycling work during the tank tests, the four pH $_{total}^{EXT}$ timeseries for SP033 (Fig. 4a) and the three pH $_{total}^{EXT}$ timeseries for SP053 (Fig. 4b) closely tracked the bottle sample pH regardless of the starting and ending salinity and the direction of salinity change. All pH $_{total}^{EXT}$ timeseries across both sensors remain tightly coupled

over Days 1 and 2 at end salinities of 18.66 and 9.60, respectively. Afterward, they all clearly diverge depending on the sensor calibration method employed on Day 3 when the sensors were switched to Tank 2 with a salinity of 1.38. Once both sensors were returned to Tank 1 at salinity 12.05 on Day 4, all pH_{total}^{EXT} timeseries across both sensors generally start to converge and tightly couple again over time and as salinity was increased to >20 on Day 5 and through the post-cycling period prior to sensor recovery.

In general, anomalies between pH_{total}^{disc} of the calibration samples and pH_{total}^{EXT}(\Delta pH_{total}) timeseries for SP033 (Fig. 5a and Table S7 in the Supplementary Materials) were tightly coupled on each day for each timeseries. In general, ΔpH_{total} for all pH_{total}^{EXT} timeseries were $<\pm 0.02$ pH on Days 1–2 and 5–6. In contrast, on Day 3 between salinities 1.38 and 1.41, ΔpH_{total} clearly diverge for the pH_{total}^{EXT} timeseries and this divergence is related to the sensor calibration method. On Day 3, ΔpH_{total} exhibits increased scatter with larger mean ΔpH_{total} for pH_{total,single}^{EXT,HC} and pH_{total,single} of 0.0244 \pm 0.0169 and - 0.0436 \pm 0.0174 pH, respectively. Increased mean ΔpH_{total} for pH_{total,single}^{EXT,HC} and pH_{total,single}^{EXT,CC} that remain closer to zero on Days 3 and 4.

For both pH $_{total,single}^{EXT,HC}$ and pH $_{total,single}^{EXT,CC}$ measured by SP033, 69.23% and 67.95% of the ΔpH_{total} values, respectively, met the GOA-ON weather-level pH data quality threshold of $<\pm0.02$ pH. In contrast, only 16.67% and 1.28% of the ΔpH_{total} values for pH $_{total,single}^{EXT,HC}$ and pH $_{total,single}^{EXT,CC}$ respectively, achieved the GOA-ON climate-level pH data quality threshold of $<\pm0.003$ pH. On the other hand, pH $_{total,split}^{EXT,HC}$ and pH $_{total,split}^{EXT,CC}$ measured by SP033 experienced better performance since 32.05% and 46.15% of the ΔpH_{total} values were $<\pm0.003$ pH, respectively, whereas 94.87% of the ΔpH_{total} values for both were $<\pm0.02$ pH.

Values of $\Delta p H_{total}$ between $p H_{total}^{disc}$ of the calibration samples and pH_{total}^{EXT} timeseries for SP053 (Fig. 5b and Table S8 in the Supplementary Materials) largely follow similar trends for SP033. Unlike SP033, however, there are only three pH_{total}^{EXT} timeseries for SP053 and $pH_{total,single}^{EXT,HC}$ and $pH_{total,split}^{EXT,CC}$ have mean ΔpH_{total} values close to zero across all six days. For $pH_{total,single}^{EXT,HC}$ measured by SP053, 51.28% and 97.44% of the ΔpH_{total} values met the GOA-ON climate-level (<±0.003 pH) and weather-level (<±0.02 pH) pH data quality thresholds, respectively. Comparably, 26.92% and 98.72% of the ΔpH_{total} values for $pH_{total,split}^{EXT,CC}$ were $<\pm0.003$ pH and $<\pm 0.02$ pH, respectively. On the other hand, pH $_{total,single}^{EXT,CC}$ has relatively larger mean $\Delta p H_{total}$ values on Days 1 and 3–6 with the greatest non-zero anomalies seen on Day 3 when the mean ΔpH_{total} was -0.0648 ± 0.0127 pH. Even more, for pH $_{total,single}^{EXT,CC}$ measured by SP053, only 7.69% and 64.10% of the $\Delta p H_{total}$ values met the GOA-ON weatherlevel and climate-level pH data quality thresholds. This analysis demonstrates that splitting out $E^{\ast}_{EXT,hc,25}$ and $E^{\ast}_{EXT,25}$ is important to achieve

Table 1 Sensor offsets (or intercepts, c_0) and sensor gains (or slopes, c_1) of model II least square fits of pH $_{\text{total}}^{\text{disc}}$ and pH $_{\text{total}}^{\text{EXT}}$ or SP033 and SP053.

Sensor	Timeseries	Sensor Offset (c_0)	Sensor Gain (c_1)
SP033	pH ^{EXT,HC} total,single pH ^{EXT,HC} total,split pH ^{EXT,CC} total,single pH ^{EXT,CC} pH _{total,single}	-0.3357 ± 0.0411 0.0129 ± 0.0239 0.3659 ± 0.0580 0.0027 ± 0.0231	$\begin{aligned} &1.0430 \pm 0.0053 \\ &0.9983 \pm 0.0031 \\ &0.9530 \pm 0.0075 \\ &0.9996 \pm 0.0030 \end{aligned}$
SP053	$\begin{array}{l} pH_{total,single}^{EXT,HC} \\ pH_{total,single}^{EXT,CC} \\ pH_{total,split}^{EXT,CC} \end{array}$	$-0.0288 \pm 0.0195 \\ 0.6739 \pm 0.0405 \\ 0.0056 \pm 0.0231$	$\begin{aligned} &1.0035 \pm 0.0025 \\ &0.9133 \pm 0.0052 \\ &0.9991 \pm 0.0030 \end{aligned}$

these pH data quality thresholds in this context when enough discrete samples are available for calibration.

5.4. Assessment of Cl-ISE performance

Unlike the long pre-deployment sensor conditioning periods (on the order of 1–2 weeks) required for the Cl-ISE noted by other studies (Bresnahan et al., 2014; Miller et al., 2018; Takeshita et al., 2021), the responses of the Cl-ISEs in both sensors were nearly instantaneous to new salinity changes in the first measurements following dilution or concentration within their 16-sec pH measurement periods. On average, after calibration, ΔpH_{total} for the first sensor measurement after salinity dilution or concentration across Days 1–6 of the tank tests for $pH_{total,split}^{EXT,HC}$ and $pH_{total,split}^{EXT,CC}$ for SP033 and $pH_{total,single}^{EXT,HC}$ and $pH_{total,split}^{EXT,CC}$ for SP053 was better than $<\pm 0.012$ pH indicating pH response was also rapid. Whereas SP033 and SP053 operated continuously in seawater for \sim 4 weeks in preparation for this work, this still sufficiently demonstrates the fast response of the Cl-ISE to rapid environmental changes in this application.

In a side-by-side comparison of the model II least square fits of pH $_{\rm total}^{\rm disc}$ and pH $_{\rm total}^{\rm EXT}$ (Table 1 and Figs. 6 and 7), the calibration method had the greatest impact on the sensor offsets (c_0) and sensor gains (c_1). Sensor offsets and sensor gains exhibited the greatest deviations from their ideal values of 0 and 1, respectively, for pH $_{\rm total,single}^{\rm EXT,HC}$ and pH $_{\rm total,single}^{\rm EXT,CC}$ for SP033 and pH $_{\rm total,split}^{\rm EXT,CC}$ for SP053. Linear fits of pH $_{\rm total,split}^{\rm EXT,HC}$ and pH $_{\rm total,split}^{\rm EXT,CC}$ for SP033 and pH $_{\rm total,split}^{\rm EXT,CC}$ for SP053 were much more robust with sensor gains and offsets substantially closer to 0 and 1, respectively. Ultimately, the single defined linear relationship between $\rm E_{EXT,hc}^*(t)$ and $\rm in~situ$ temperature for SP053 provided a robust linear fit for pH $_{\rm total,single}^{\rm EXT,HC}$ for SP053.

The RMSEs calculated from the model II least square fits between $pH_{total}^{disc} \ and \ pH_{total,split}^{EXT,HC} \ and \ pH_{total,split}^{EXT,CC} \ for \ SP033 \ and \ between \ pH_{total}^{disc} \ and$ $pH_{total,single}^{EXT,CC} \ and \ pH_{total,split}^{EXT,CC} \ for \ SP053 \ (Table \ 2) \ are \ accurate \ to \le \pm 0.02 \ pH$ relative to pH_{total}^{disc} across all salinities. Therefore, pH_{total}^{EXT} measured using the Cl-ISE as the reference electrode meets the GOA-ON weather-level data quality threshold on the short timescales of this work. Further, timeseries on Days 1–2 and 4–6 are also accurate to $\leq \pm 0.01$ pH relative to $pH_{total}^{disc}.$ In contrast, RMSEs between pH_{total}^{disc} and the selected $\ pH_{total}^{EXT}$ for Day 3 at salinity ${\sim}1.38\text{--}1.39$ and $pH^{disc}_{total} < 7.2$ were always higher (but still better than $\leq \pm 0.02$ pH relative to pH $_{total}^{disc}$). The reduced accuracy for Day 3 is not surprising given that the physicochemical characterization of purified mCP dye used to calculate pHEXT from Müller and Rehder (2018) is less reliable at salinity <5 where pH of the TRIS buffers used to perform the dye characterization is not accurately known (Müller et al., 2018) and at pH < 7.2 where is mCP is not typically used to measure pH (Liu et al., 2011). On Day 3, the tank test waters with TA $<125\;\mu\text{mol}$ kg⁻¹ were more poorly buffered which potentially introduced an equilibration issue between the electrodes and overlying waters throughout the six-hour sampling period that may have increased scatter and reduced accuracy. Also, discrete bottle samples for pH^{disc}_{total} were collected unfiltered, so impacts of particles on spectrophotometric pH measurements may also contribute here. Still, depending on water budgets and logistical constraints, filtering discrete water samples during collection would eliminate these potential impacts in future work. Given the excellent agreement between pH_{total}^{EXT} and pH_{total}^{disc} across all other days; however, this likely does not represent a substantial contribution. RMSEs were not calculated and reported for $pH_{total,single}^{EXT,HC}$ and $pH_{total,single}^{EXT,CC}$ for SP033 and $pH_{total,single}^{EXT,CC}$ for SP053.

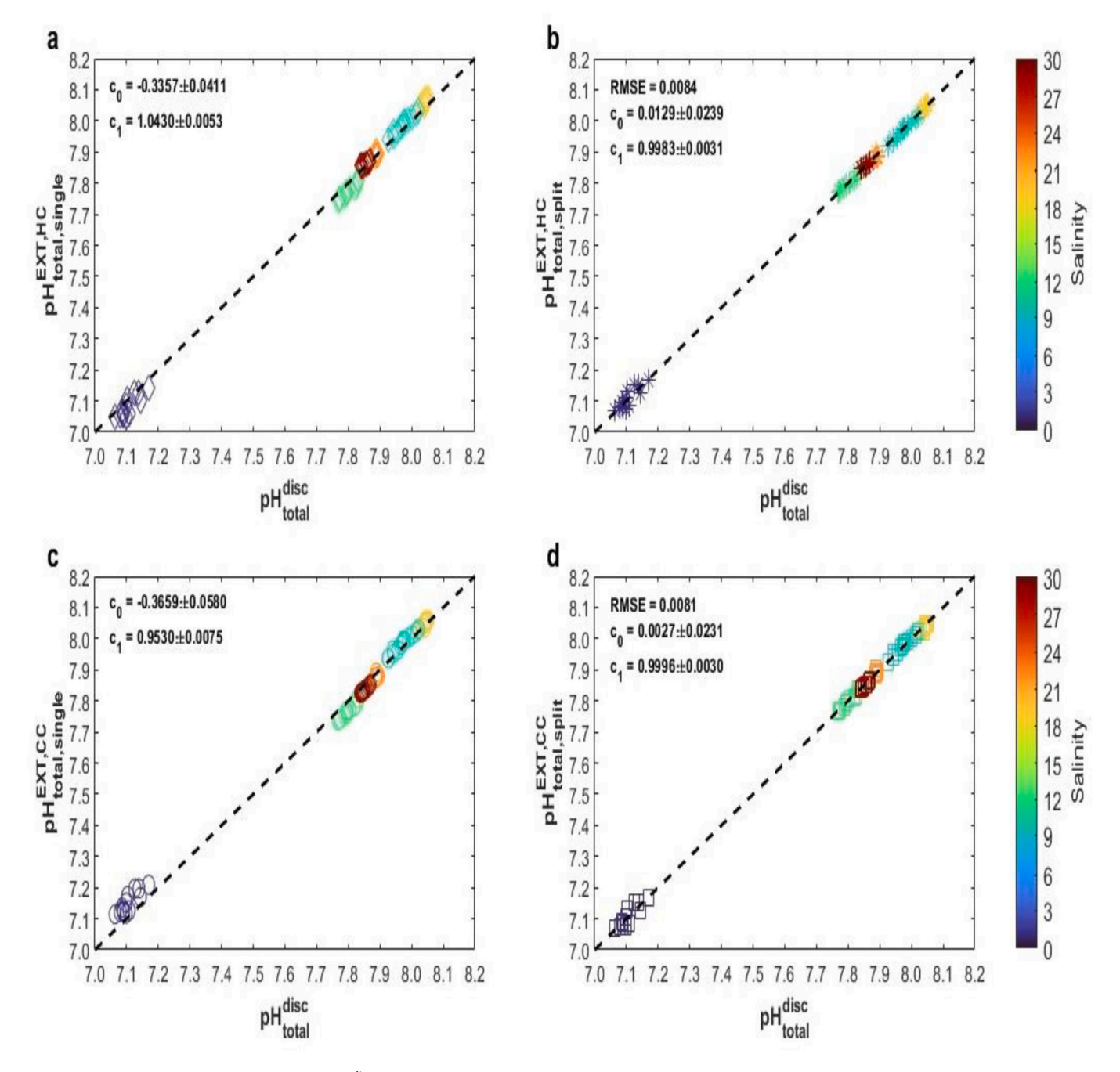


Fig. 6. Property-property plots of pH_{total}^{EXT} versus pH_{total}^{disc} of the calibration samples for SP033 as a function of salinity (color-coded). Dashed black lines represent a 1:1 relationship ($pH_{total}^{EXT} = pH_{total}^{disc}$). RMSEs were not calculated for $pH_{total,single}^{EXT,HC}$ or $pH_{total,single}^{EXT,CC}$. Please see Table 1 for descriptions of the comparisons.

5.5. Primary and secondary corrections for pH_{total}

To calculate pH when using the Cl-ISE as the reference electrode, primary corrections to account for variable temperature are employed via the Nernst slopes for both reaction approaches. In addition, $\gamma_H\gamma_{Cl}m_{Cl}$ and $^\kappa\gamma_{Cl}\kappa_{Cl}$ are employed during calibration as primary corrections for the complete cell and half-cell reaction approaches, respectively, to account for variable temperature and salinity. However, $\gamma_H\gamma_{Cl}$ from Khoo et al. (1977) must be extrapolated down from salinity 20 to calculate E^*_{EXT} on the free scale. Typically, the ion activity coefficient defined by the Davies convention (e.g., Stumm and Morgan (1996)) must be extrapolated up from I=0.5 (nominally salinity 25), but when the dielectric constant (ϵ) is considered as a function of temperature and

salinity rather than temperature alone, the Davies convention for $^\kappa\gamma_{Cl}$ is extended to $I\leq 0.7$ (please see Figs. S1 and S2 in the Supplementary Materials) and allows the calculation of $E^*_{EXT,hc}$ on the total scale during calibration.

Both E_{EXT}^* and $E_{EXT,hc}^*$ (and the final calculated pH $_{total}^{EXT}$) are benchmarked to pH $_{total}^{disc}$ which replaces the standard buffer solutions that were originally used to determine $\gamma_H\gamma_{Cl}$ and $^\kappa\gamma_{Cl}$ as the primary pH standard. Nevertheless, purified mCP dye characterizations used to determine pH $_{total}^{disc}$ are traceable to primary TRIS buffer standards (Müller et al., 2018). Therefore, when using pH $_{total}^{disc}$ to calculate $E_{EXT,hc,25}^*$ and $E_{EXT,25}^*$, it is possible to normalize the effects of non-idealities associated with extending $\gamma_H\gamma_{Cl}$ and $^\kappa\gamma_{Cl}$ beyond their optimized salinity ranges to calculate an accurate final pH $_{total}^{EXT}$. Together with the updated Davies

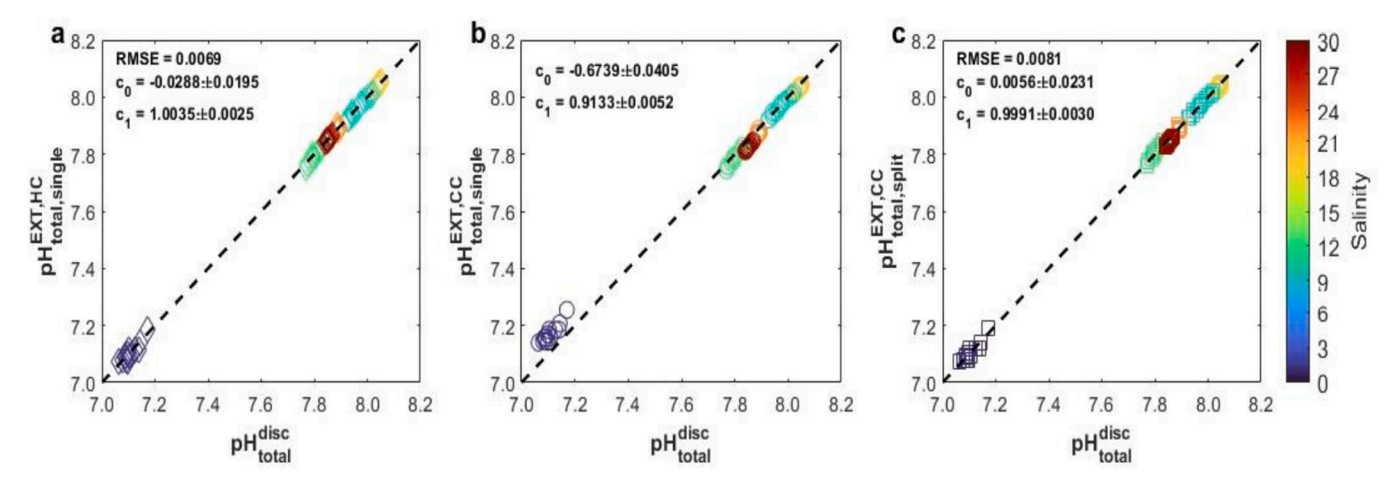


Fig. 7. Property-property plots of pH_{total}^{EXT} versus pH_{total}^{disc} of the calibration samples for SP053 as a function of salinity (color-coded). Dashed black lines represent a 1:1 relationship ($pH_{total}^{EXT} = pH_{total}^{disc}$). A RMSE was not calculated for $pH_{total,single}^{EXT,CC}$. Please see Table 1 for descriptions of the comparisons.

 $\label{eq:table 2} \textbf{Root-mean square errors calculated from model II least square fits for select comparisons of PH_{total}^{disc} and PH_{total}^{EXT} for $P033$ and $P9053$ using the calibration samples that were collected on each day (Days 1–6) and for all the calibration samples that were collected during all days of the tank tests (All).}$

Day	SP033	SP033		SP053	
	pH _{total,split}	pH ^{EXT,CC} _{total,split}	pH ^{EXT,HC} _{total,single}	$pH_{total,split}^{EXT,CC}$	
	RMSE	RMSE	RMSE	RMSE	
1	0.0053	0.0053	0.0032	0.0043	
2	0.0058	0.0054	0.0048	0.0056	
3	0.0162	0.0168	0.0123	0.0122	
4	0.0048	0.0049	0.0080	0.0096	
5	0.0066	0.0050	0.0049	0.0057	
6	0.0057	0.0026	0.0029	0.0084	
All	0.0084	0.0081	0.0069	0.0081	

equation calculations, these primary corrections are well supported for $^\kappa\gamma_{Cl}$ using the half-cell reaction approach to $I\leq 0.7$ for SP053 by a single robust linear relationship between $E_{EXT,hc}^*(t)$ and in situ temperature. Our analysis suggests that extrapolating $\gamma_H\gamma_{Cl}$ on the free scale down to salinity <20 for the complete cell reaction approach is only dependable down to salinity $\sim\!9.6-9.7$ for SP053. At our lowest salinity, the E_{EXT}^* deviation is likely due to the changing difference between the free and total scales in response to changes in $\left[SO_4^{2-}\right]_{total}$ and K_S with salinity during E_{EXT}^* calculation on the free scale. This is apparent from the Day 3 relationship between $E_{EXT}^*(t)$ and in situ temperature at salinity $\sim\!1.38-1.40$ that was positively shifted for both sensors relative to those of Days 1–2 and 4–6, as shown in Fig. S8a-b in the Supplementary

After calibration, our results still differed from our understanding of electrode response based on *in situ* field deployments. Here, this manifested in the occurrence of multiple distinct linear relationships between $E_{\rm EXT,hc}^*(t)$ or $E_{\rm EXT}^*(t)$ and *in situ* temperature and multiple distinct temporal clusters of $E_{\rm EXT,hc,25}^*$ or $E_{\rm EXT,25}^*$ over different salinity conditions. Our present findings have not been previously described in field deployments in nearshore waters, likely due to the lack of discrete samples for sensor calibration and validation. These issues may be caused by the following either singly or in combination – (a) response issues with the Cl-ISE as the reference electrode and/or the ISFET as the H^+ -sensitive measuring electrode, (b) use of $^\kappa\gamma_{\rm Cl}$ versus $\gamma_{\rm H}\gamma_{\rm Cl}$, (c) calculating $E_{\rm EXT,bc}^*$ and $E_{\rm EXT}^*$ on the total and free scales, respectively,

due to changes in $\left[SO_4^2^-\right]_{total}$ and K_S between salinity 1 and 31, and (d) inter-sensor variability between SP033 and SP053. Further work is needed to determine which of these issues are most important and when. Nonetheless, we accounted for some of this by splitting $E_{EXT,hc,25}^*$ and $E_{EXT,25}^*$ based on salinity and then calculating and applying independent average $E_{EXT,hc,25}^*$ or $E_{EXT,25}^*$ to each segment. Ultimately, by splitting out these calibrations, the final calculated pH $_{total}^{EXT}$ and pH $_{total}^{disc}$ approached parity

Whereas splitting out and applying $E_{EXT,hc,25}^*$ and $E_{EXT,25}^*$ based on salinity deviates from established Sensor Best Practices, its feasibility is demonstrated in the fit parameters of the Modell II least square fits of $pH_{total,split}^{EXT}$ and pH_{total}^{disc} (Table 2 and Figs. 6 and 7) discussed in section 5.4. Even more, the tighter agreement of $\Delta p H_{total}$ between $p H_{total,split}^{EXT}$ and pH_{total}^{disc} relative to $pH_{total,single}^{EXT}$ and pH_{total}^{disc} (Fig. 5a-b) further demonstrate the efficacy of this new calibration method. In this context, this new multi-point in situ or field calibration provides a superior means of minimizing the anomaly between the sensor pH and the discrete sample pH as needed in our application. We were only able to accomplish this since we had a high number of high-quality discrete samples that covered an extensive salinity range. Accordingly, this alternative calibration method will likely need to be refined before widespread application to field data or may not be possible in field settings since discrete sample collection in the field is challenging and demands substantial time and resources.

The best data from this work in terms of lowest RMSE from robust Model II least square fit parameters and lowest ΔpH_{total} comes from $pH_{total,single}^{EXT,HC}$ for SP053. Here, $E_{EXT,hc,25}^*$ values were stable across all salinities and data were able to be recalibrated using a single average $E_{EXT,hc,25}^*$ based on all calibration samples regardless of salinity. Therefore, this remains the preferred calibration method independent of reaction approach whenever possible, as defined by current Sensor Best Practices (e.g., Bresnahan et al., 2014).

5.6. Implications for field deployments in nearshore systems

The overall excellent agreement between pH_{total} and pH_{disc} across all salinity steps differed from the results of limited *in situ* field deployments of Durafet-based pH sensors in dynamic tidally forced nearshore systems over similar environmental conditions. Field studies demonstrated pH_{total} calculated using the complete cell reaction approach to be less reliable with higher uncertainties in those settings (Fritzsche et al., 2018; Gonski et al., 2018, 2023). Whereas the results of this work

contrast with those *in situ* field deployments, there are several notable differences between the work presented here and those *in situ* field studies. Here, only a single large rapid salinity change to simulate tidal mixing was performed each day, and the sensors were given ~ 24 h to equilibrate to new environmental conditions.

In tidally-forced nearshore systems, however, salinities consistently change with tidal mixing between every measurement, so the equilibration and/or conditioning time sensors have for each new pH, temperature, and salinity in the field is only as long as the sensor's sampling interval (e.g., 30 min). Our work was also performed using clean seawater and DI water and operated as a simplified dilution and concentration experiment. In contrast, concentrations of major and minor ions likely deviate from seawater conservative ratios in freshwater endmembers of real nearshore systems and are also characterized by high turbidity that may affect in situ electrode response (Gonski et al., 2018, 2023). Moreover, the water chemistry of natural waters in nearshore systems will also differ from those conditions experienced during the tank tests and may include other anions such as bromide (Br-) and sulfide (S^{2-}) at higher concentrations and at different ratios to salinity relative to seawater. High levels of humics or organics from salt marsh and/or wastewater treatment plant inputs may also be present and negatively impact the Cl-ISE response (Gonski et al., 2023).

Notably, the divergence between linear relationships $E_{EXT,hc}^*(t)$ or $E_{EXT}^{*}(t)$ and in situ temperature was larger for SP033 relative to SP053 given that their Cl-ISEs were installed at different times (~4 months before for SP033 and ~ 11 days before for SP053) even though they were stored and/or operated in seawater prior to testing. If we were to generalize the inconsistent electrode response to new salinities exhibited by SP033 as a sensor that has been deployed in a dynamic nearshore environment for >4-6 months and the repeatable electrode response to new salinities exhibited by SP053 as a sensor that was newly deployed, then this divergence may grow over time. Ultimately, this work highlights the need for high-frequency reference pH data to track electrode response in dynamic nearshore systems, that spans its full ranges of salinity and rates of salinity change through the deployment of colocated redundant pH sensors, use of empirical regional marine carbonate system relationships, and/or collection of plentiful discrete bottle samples.

6. Conclusions

Here, we defined a half-cell reaction approach to calculate pH_{total}^{EXT} using the electrochemical couple comprised of the Cl-ISE (reference electrode) and the ISFET of the Honeywell Durafet (H $^+$ -sensitive measuring electrode). This approach differed from the complete cell reaction approach defined by Martz et al. (2010) (where the responses of both electrodes are combined) by splitting out and isolating the independent responses of the Cl-ISE to Cl $^-$ (and salinity) and the ISFET to H $^+$ (and pH). In contrast to the complete cell reaction approach, the half-cell reaction approach enabled the dependence of pH $_{total}^{EXT}$ on $^{\kappa}\gamma_{Cl}\kappa_{Cl}$ and $^{\kappa}\gamma_{H}$ to be accounted for via Eqs. (9a) and (17), respectively; thus, allowing sensor calibration and pH calculation to be carried out directly on the total scale.

Moreover, we calculate $^\kappa\gamma_{Cl}$ using the Davies convention (Eq. (25)) on a molinity (or mol (kg-soln) $^{-1}$) basis (as described in section 2.2.2 and section S2 in the Supplementary Materials) for the half-cell reaction approach. In contrast, $\gamma_H\gamma_{Cl}$ for the complete cell reaction approach is only a function of temperature (Khoo et al., 1977) and is calculated in molality units (mol (kg-H₂O) $^{-1}$) (Bresnahan et al., 2014; Martz et al., 2010). We further applied and assessed the suitability of both reaction approaches for pH calculation using Cl-ISE measurements made using two SeapHOx sensors over a six-day period in a test tank when salinity and pH were decreased and increased between 1 and 31 and 6.9 and 8.1, respectively.

The response of the Cl-ISE to new salinity changes during the first

sensor measurements following salinity dilution and concentration was rapid, and calculations showed sensor pH was within ≤±0.012 pH of pH^{disc}, on average, across all salinities for both sensors. Further, the sensor pH values calculated using the Cl-ISE as the reference electrode were accurate to <±0.02 pH at all salinities for both sensors thereby meeting the GOA-ON weather-level pH data quality threshold. Therefore, the Cl-ISE as the reference electrode is suitable for calculating and reporting pH with the accuracy needed to help detect local spatial patterns and short-term variations in acidification in dynamic nearshore waters. Our work shows that both electrode reaction approaches are reliable, have unique benefits, and thus, are an example of Hess' Law that states the thermodynamics of the system is independent of the reaction pathway from the initial to the final state (Sandler and Woodcock, 2010). As a result, we now have a second independent approach to calculate pHEXT using the Cl-ISE as the reference electrode that can be reported in addition to the complete cell reaction approach and utilized as an additional mode of data quality control for future in situ field sensor deployments.

We employed a new sensor calibration method whereby we split out the data for $E^*_{EXT,hc,25}$ and $E^*_{EXT,25}$ and independently calibrated the corresponding segments of their pH sensor timeseries according to salinity as needed. When compared with using single average values of $E^*_{EXT,hc,25}$ or $E^*_{EXT,25},$ splitting out the data for $E^*_{EXT,hc,25}$ and $E^*_{EXT,25}$ based on salinity improves Model II least square fits between pHEXT total.split and pH^{disc}_{total} and broadly improves their accuracy across all salinities. Nevertheless, additional work in natural waters of salinity <1.5 with higher alkalinity and buffering capacity (e.g., relative to TA $< 125 \mu mol \text{ kg}^{-1}$ as seen here on Day 3 at salinity 1.38-1.41) and between salinities 1 and 10 with finer salinity incrementation than seen here with the half-cell and complete cell reaction approaches is needed. Additional work with the half-cell reaction approach at temperatures <20°C is also needed. Since ion activity coefficients are also pressure-dependent, additional work addressing pressure compensation for the half-cell reaction approach is needed before it can be utilized in water column profiling applications (e.g., Deep-Sea Durafet described in Johnson et al. (2016)).

Based on the results presented here that contrast with the results of the few *in situ* field deployments of Durafet-based pH sensors in dynamic tidally-forced nearshore system under similar environmental conditions, we do not yet fully understand *in situ* electrode response over the full environmental ranges of natural waters. Therefore, future work should examine the effects of stimuli external to the correction of variable temperature and salinity conditions on pH calculation using the Cl-ISE as the reference electrode like those described in section 5.6 including the impacts of interfering anions (e.g., Br $^-$ and S $^{2-}$) and humics that are present at higher concentrations in nearshore waters relative to seawater. Whereas past work has predominantly focused on the responses of the Durafet's reference electrodes, further scrutiny of the response of the ISFET as the H $^+$ -sensitive measuring electrode is also needed.

CRediT authorship contribution statement

S. Fisher Gonski: Writing – review & editing, Writing – original draft, Visualization, Validation, Supervision, Project administration, Methodology, Investigation, Formal analysis, Data curation, Conceptualization. George W. Luther: Writing – review & editing, Writing – original draft, Visualization, Validation, Supervision, Resources, Methodology, Investigation, Formal analysis, Data curation, Conceptualization. Amanda L. Kelley: Writing – review & editing, Writing – original draft, Validation, Methodology, Investigation. Todd R. Martz: Writing – review & editing, Validation, Investigation. Elliott G. Roberts: Writing – review & editing, Validation, Investigation, Formal analysis, Data curation. Xinyu Li: Writing – review & editing, Validation, Investigation, Formal analysis, Data curation. Bo Dong: Writing – review &

editing, Validation, Investigation, Formal analysis, Data curation. Jordan A. Watson: Writing – review & editing, Validation, Investigation, Formal analysis, Data curation, Conceptualization. Taylor S. Wirth: Writing – review & editing, Validation, Investigation. Najid Hussain: Writing – review & editing, Validation, Investigation, Formal analysis, Data curation. Randy J. Feris Serrano: Writing – review & editing, Validation, Investigation. Edward Hale: Writing – review & editing, Supervision, Resources. Wei-Jun Cai: Writing – review & editing, Validation, Supervision, Resources, Funding acquisition.

Data availability

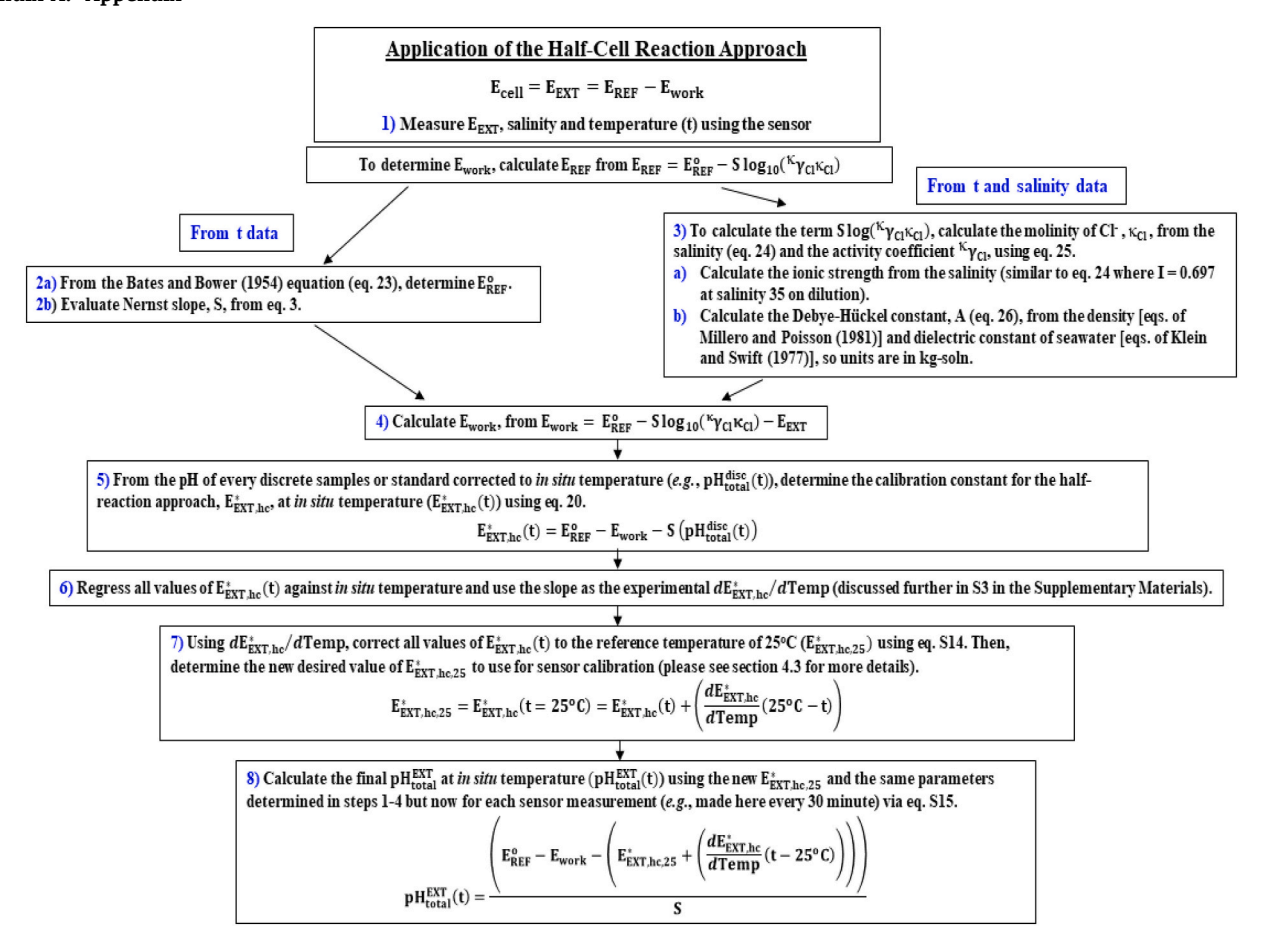
The data that has been used is confidential.

Acknowledgements

We sincerely thank Kenneth S. Johnson and Yuichiro Takeshita of

Monterey Bay Aquarium Research Institute for their insights and support and Ben Freiberger of Scripps Institution of Oceanography for his assistance with refurbishing the two SeapHOx sensors used in this work. We sincerely thank Jonathan Harp from CHPT Manufacturing, Inc. for his help with sensor modifications, and the staff of University of Delaware's Lewes Campus Maintenance and Operations for providing logistical support with preparing for and conducting the tank tests described herein. Finally, we thank two anonymous reviewers and the Associate Editor for their helpful comments that greatly improved the manuscript. Financial support for this work was provided by a National Science Foundation EPSCoR Grant (1757353) and the State of Delaware to the University of Delaware with a sub-grant awarded to Wei-Jun Cai. Support for S. F. Gonski was also provided by the University of Delaware Graduate College through the Doctoral Fellowship for Excellence.

Appendix A. Appendix



Appendix 1. Flow chart to determine parameters from the half-cell reaction approach.

Appendix B. Supplementary data

Supplementary data to this article can be found online at https://doi.org/10.1016/j.marchem.2024.104373.

References

- Alberty, R.A., Daniels, F., 1979. Physical Chemistry, 5th ed. John Wiley & Sons. Bagshaw, E.A., Wadham, J.L., Tranter, M., Beaton, A.D., Hawkings, J.R., Lamarche-Gagnon, G., Mowlem, M.C., 2021. Measuring pH in low ionic strength glacial meltwaters using ion selective field effect transistor (ISFET) technology. Limnol. Oceanogr. Methods 19 (3), 222–233.
- Bakker, E., Pretsch, E., 2007. Modern potentiometry. Angew. Chem. Int. Ed. 46 (30), 5660–5668.
- Bard, A.J., Faulkner, L.R., 2001. Electrochemical Methods: Fundamentals and Applications, 2nd ed. John Wiley & Sons.
- Bates, R.G., Bower, V.E., 1954. Standard potential of the silver-silver-chloride electrode from 0 to 95°C and the thermodynamic properties of dilute hydrochloric acid solutions. J. Res. Natl. Bur. Stand. 53, 283–290.
- Bresnahan, P.J., Martz, T.R., Takeshita, Y., Johnson, K.S., LaShomb, M., 2014. Best practices for autonomous measurements of seawater pH with the Honeywell Durafet. Methods in Oceanography 9, 44–60.
- Bresnahan, P.J., Wirth, T.R., Martz, T.R., Anderssen, A.J., Cyronak, T., D'Angelo, S., Pennise, J., Melville, W.K., Lenain, L., Statom, N., 2016. A sensor package for mapping pH and oxygen from mobile platforms. Methods in Oceanography 17, 1–13.
- Bresnahan, P.J., Takeshita, Y., Wirth, T., Martz, T.R., Cyronak, T., Albright, R., et al., 2021. Autonomous in situ calibration of ion-sensitive field effect transistor pH sensors. Limnology and Oceanography: Methods 19 (2), 132–144.
- Chai, F., Johnson, K.S., Claustre, H., Xing, X., Wang, Y., Boss, E., et al., 2020. Monitoring ocean biogeochemistry with autonomous platforms. Nature Reviews Earth & Environment 1 (6), 315–326.
- Clegg, S.L., Whitfield, M., 1991. Activity coefficients in natural waters. In: Pitzer, K.S. (Ed.), Activity Coefficients in Electrolyte Solutions, 2nd ed. CRC Press, pp. 279–434.
- Dickson, A.G., 1990. Standard potential of the reaction: AgCl (s) + 1/2 H₂ (g) = Ag(s) + HCl (aq), and the standard acidity constant of the ion HSO $_4^-$ in synthetic sea water from 273.15 to 318.15 K. J. Chem. Thermodyn. 22 (2), 113–127.
- Dickson, A.G., Sabine, C.L., Christian, J.R., 2007. Guide to Best Practices for Ocean ${\rm CO}_2$ Measurements.
- Duke, P.J., Else, B.G.T., Jones, S.F., Marriot, S., Ahmed, M.M.M., Nandan, V., et al., 2021. Seasonal marine carbon system processes in an Arctic coastal landfast ice environment observed with an innovative sensor platform. Elementa: Science of the Anthropocene 9 (1), 00103.
- Fritzsche, E., Staudinger, C., Fischer, J.P., Thar, R., Jannasch, H.W., Plant, J.N., et al., 2018. A validation and comparison study of new, compact, versatile optodes for oxygen, pH and carbon dioxide in marine environments. Mar. Chem. 207, 63–76.
- Gonski, S.F., Cai, W.-J., Ullman, W.J., Joesoef, A., Main, C.R., Pettay, D.T., Martz, T.R., 2018. Assessment of the suitability of Durafet-based sensors for pH measurement in dynamic estuarine environments. Estuar. Coast. Shelf Sci. 200, 152–168.
- Gonski, S.F., Ullman, W.J., Pettay, D.T., Booksh, K.S., Martz, T.R., Luther III, G.W., Cai, W.-J., 2023. Understanding the Dynamic Response of Durafet-Based Sensors: A Case Study from the Murderkill Estuary-Delaware Bay System (Delaware, USA). Estuarine, Coastal and Shelf Science, p. 108247.
- Johnson, K.S., Jannasch, H.W., Coletti, L.J., Elrod, V.A., Martz, T.R., Takeshita, Y., Carlson, R.J., Connery, J.G., 2016. Deep-Sea DuraFET: a pressure tolerant pH sensor designed for global sensor networks. Anal. Chem. 88 (6), 3249–3256.
- Khalsa, N.S., Gatt, K.P., Sutton, T.M., Kelley, A.L., 2021. Characterization of the abiotic drivers of abundance of nearshore Arctic fishes. Ecol. Evol. 11 (16), 11491–11506.
- Khoo, K.H., Ramette, R.W., Culberson, C.H., Bates, R.G., 1977. Determination of hydrogen ion concentrations in seawater from 5 to 40°C: standard potentials at salinities from 20 to 45. Anal. Chem. 49 (1), 29–34.
- Klein, L.A., Swift, C.T., 1977. An improved model for the dielectric constant of sea water at microwave frequencies. IEEE Trans. Antennas Propag. 25 (1), 104–111.
- Liu, X., Patsavas, M.C., Byrne, R.H., 2011. Purification and characterization of metacresol purple for spectrophotometric seawater pH measurements. Environ. Sci. Technol. 45 (11), 4862–4868.
- Martz, T.R., Connery, J.G., Johnson, K.S., 2010. Testing the Honeywell Durafet for seawater pH applications. Limnology & Oceanography: Methods 8, 172–184.
- McLaughlin, K., Dickson, A., Weisberg, S.B., Coale, K., Elrod, V., Hunter, C., et al., 2017. An evaluation of ISFET sensors for coastal pH monitoring applications. Reg. Stud. Mar. Sci. 12, 11–18.
- Miller, C.A., Kelley, A.L., 2021. Seasonality and biological forcing modify the diel frequency of nearshore pH extremes in a subarctic Alaskan estuary. Limnol. Oceanogr. 2021, 1–17.

- Miller, C.A., Pocock, K., Evans, W., Kelley, A.L., 2018. An evaluation of the performance of sea-bird Scientific's SeaFET autonomous pH sensor: considerations for the broader oceanographic community. Ocean Sci. 14, 751–768.
- Miller, C.A., Bonsell, C., McTigue, N.D., Kelley, A.L., 2021. The seasonal phases of an Arctic lagoon reveal the discontinuities of pH variability and CO₂ flux at the air–sea interface. Biogeosciences 18 (3), 1203–1221.
- Millero, F.J., Poisson, A., 1981. International one-atmosphere equation of state of seawater. Deep Sea Research Part A. Oceanographic Research Papers 28 (6), 625–629.
- Millero, F.J., Graham, T.B., Huang, F., Bustos-Serrano, H., Pierrot, D., 2006. Dissociation constants of carbonic acid in seawater as a function of salinity and temperature. Mar. Chem. 100 (1), 80–94.
- Millero, F.J., Feistel, R., Wright, D.G., McDougall, T.J., 2008. The composition of standard seawater and the definition of the reference-composition salinity scale. Deep-Sea Res. I Oceanogr. Res. Pap. 55 (1), 50–72.
- Mowlem, M., Beaton, A., Pascal, R., Schaap, A., Loucaides, S., Monk, S., et al., 2021. Industry partnership: lab on chip chemical sensor technology for ocean observing. Front. Mar. Sci. 1407.
- Mucci, A., Levasseur, M., Gratton, Y., Martias, C., Scarratt, M., Gilbert, D., et al., 2018. Tidally induced variations of pH at the head of the Laurentian Channel. Can. J. Fish. Aquat. Sci. 75 (7), 1128–1141.
- Müller, J.D., Rehder, G., 2018. Metrology of pH measurements in brackish waters—Part 2: experimental characterization of purified meta-cresol purple for spectrophotometric pH_T measurements. Front. Mar. Sci. 5, 177.
- Müller, J.D., Bastkowski, F., Sander, B., Seitz, S., Turner, D.R., Dickson, A.G., Rehder, G., 2018. Metrology for pH measurements in brackish waters—Part 1: extending electrochemical pH_T measurements of TRIS buffers to salinities 5–20. Front. Mar. Sci. 5, 176.
- Nehir, M., Esposito, M., Loucaides, S., Achterberg, E.P., 2022. Field application of automated spectrophotometric analyzer for high-resolution in situ monitoring of pH in dynamic estuarine and coastal waters. Front. Mar. Sci. 9, 891876.
- Newton, J.A., Feely, R.A., Jewett, E.B., Williamson, P., Mathis, J., 2015. Global Ocean Acidification Observing Network: Requirement and Governance Plan, 2nd ed. GOA-ON
- Okazaki, R.R., Sutton, A.J., Feely, R.A., Dickson, A.G., Alin, S.A., Sabine, C.L., Bunje, P. M.E., Virmani, J.I., 2017. Evaluation of marine pH sensors under controlled and natural conditions for the Wendy Schmidt Ocean Health XPRIZE. Limnology and Oceanography: Methods 15 (6), 586–600.
- Peltzer, E., 2007. Model II least squares fit: lsqfitma.m. http://www3.mbari.org/ Products/Matlab shell scripts/regress/lsqfitma.m.
- Pettay, D.T., Gonski, S.F., Cai, W.-J., Sommerfield, C.K., Ullman, W.J., 2020. The ebb and flow of protons: a novel approach for the assessment of estuarine and coastal acidification. Estuar. Coast. Shelf Sci. 236, 106627.
- Saba, G.K., Wright-Fairbanks, E., Chen, B., Cai, W.-J., Barnard, A.H., Jones, C.P., Miles, T., 2019. The development and validation of a profiling glider deep ISFETbased pH sensor for high resolution observations of coastal and ocean acidification. Front. Mar. Sci. 6, 664.
- Sandler, S.I., Woodcock, L.V., 2010. Historical observations on laws of thermodynamics. J. Chem. Eng. Data 55, 4485–4490.
- Sastri, A., Christian, J.R., Achterberg, E.P., Atamanchuk, D., Buck, J.J.H., Bresnahan, P. J., et al., 2019. Perspectives on in situ sensors for ocean acidification research. Front. Mar. Sci. 6, 653.
- Sharp, J.D., Pierrot, D., Humphreys, M.P., Epitalon, J.M., Orr, J.C., Lewis, E.R., 2020. CO2SYSv3 for MATLAB (Version v3. 2.0). Zenodo. Available online at: https://zenodo.org/record/4774718#.YWRThxBBw7w.
- Stumm, W., Morgan, J.J., 1996. Aquatic Chemistry: Chemical Equilibria and Rates in Natural Waters, 3rd ed. Wiley-Interscience.
- Takeshita, Y., Martz, T.R., Johnson, K.S., Dickson, A.G., 2014. Characterization of an ion-selective field effect transistor and chloride ion-selective electrodes for pH measurements in seawater. Anal. Chem. 86 (22), 1189–1195.
- Takeshita, Y., Jones, B.D., Johnson, K.S., Chavez, F.P., Rudnick, D.L., Blum, M., et al., 2021. Accurate pH and $\rm O_2$ measurements from spray underwater gliders. J. Atmos. Oceanic Tech. 38 (2), 181–195.
- Uppström, L.R., 1974. The boron/chlorinity ratio of deep-sea water from the Pacific Ocean. Deep Sea Res. 21, 161–162.
- Velo, A., Padin, X.A., 2022. Advancing real-time pH sensing capabilities to monitor coastal acidification as measured in a productive and coastal estuary (*Ría de Arousa*, NW Spain). Front. Mar. Sci. 9, 941359.